

**Roska Tamás Doctoral School of Sciences and Technology
Faculty of Information Technology and Bionics
Pázmány Péter Catholic University**

Balázs Gábor Dombovári

**IN VIVO VALIDATION AND SOFTWARE
CONTROL OF ACTIVE INTRACORTICAL
MICROELECTRODES**

Ph.D. DISSERTATION

Scientific advisor:

István Ulbert



Budapest, 2016

To my loving wife, son, parents and family

Table of Contents

1	List of abbreviations	6
2	List of figures	8
3	List of tables	11
4	Abstract.....	12
5	Introduction	14
5.1	Preface	14
5.2	Recent applications of neural devices	15
5.3	Brain stimulation and neural activity recording	16
6	Cortical neural circuitry	17
6.1	Neuroanatomy of the brain	17
6.2	Mechanical properties of brain tissue	18
6.3	Brain micromotions	19
6.4	Action potential generation	19
6.5	Propagation of the action potential	21
6.6	Non-invasive recording methods.....	21
6.7	Invasive recording methods.....	22
6.7.1	Extracellular recording techniques	23
6.7.2	Intracellular recording techniques	23
6.8	Origins of the brain electrical signal.....	24
7	Properties of sleep	26
7.1	Sleep – in general	26
7.2	Sleep stages	27
7.3	Slow wave sleep and slow oscillations.....	28
7.4	Generators of the slow oscillation	30
7.5	Reactive properties of sleep.....	32
8	Advances in electrode fabrication	33
8.1	From hand assembled electrodes to MEMS based probes	33
8.2	Utah Electrode Array.....	33

8.3	Michigan Probe	34
8.4	NeuroProbes and Caltech Probes	35
8.5	Mechanical adjustment of electrode position	35
9	Objectives	37
10	Electronic depth control concept	38
10.1	Gliosis and biocompatibility	38
10.2	Electronic depth control probe	39
11	Electronic depth control software – NeuroSelect	41
11.1	Graphical user interface	41
11.2	Programming environment	42
11.3	Programming features	43
11.4	NeuroSelect Programming Introduction	46
11.4.1	Data Structure of NeuroSelect Software	46
11.4.2	wxWidgets	50
11.4.3	Anthemion DialogBlocks	50
11.4.4	Subversion	51
11.4.5	Doxygen	51
11.5	Data acquisition	52
11.6	Electrode selection	52
11.6.1	Manual electrode selection mode	52
11.6.2	Semi-automatic electrode selection mode	53
11.7	Data saving	55
11.8	SNR metric for spike quality assessment per channel	55
11.9	Perspectives of future developments	56
12	Neural signal processing	57
12.1	Spike sorting and clustering	57
12.1.1	Threshold detection	59
12.1.2	Differentiating spikes	59
12.1.3	Clustering algorithms	60

12.1.3.1	K-means based clustering	60
12.1.3.2	Bayesian clustering	60
12.1.3.3	Expectation maximization clustering	61
12.1.4	Open problems in spike sorting practice	62
12.2	Fourier and wavelet transformations	62
12.2.1	Displaying biological signals	62
12.2.2	Fast Fourier Transformation	63
12.2.3	Wavelet transformation	64
12.2.4	Spectrogram for state locked changes in EEG	65
13	Biological results	66
13.1	General remarks	66
13.2	Implantation procedures	66
13.3	Neural data recording procedures	67
13.4	Temporal, spectral, and spatial properties of the SO	68
13.5	Detection of up- and down-states	69
13.6	Averaged depth profiles of the SO	70
13.7	Properties of SUA	72
13.7.1	Firing patterns of single unit activities	74
14	Conclusions	75
15	Novel scientific results	77
16	Acknowledgements	79
17	Publications	80
17.1	Author's publications related to the dissertation	80
17.2	Authors' other publications not related to the dissertation	80
17.3	Authors conference posters	81
18	References	83

1 List of abbreviations

AASM - American Academy of Sleep Medicine

AEP – Auditory Evoked Potential
AP – Action Potential

BMI – Brain Machine Interface

BOLD - Blood Oxygenation Level Dependent

CMOS - Complementary Metal-Oxide Semiconductor

CT - Computer Tomography

DAQ – Data Acquisition

DFT – Discrete Fourier Transformation

DRIE – Deep Reactive Ion Etching

DWT – Discrete Wavelet Transformation

EDC – Electronic Depth Control

EDF – European Data Format

EEG – Electroencephalogram

ECoG - Electrocorticographic

EM – Expectation Maximization

EPSP – Excitatory Postsynaptic Potential

ERP – Event Related Potential

EAP - Extracellular Action Potential

FFT - Fast Fourier Transformation

fMRI – functional MRI

FT – Fourier Transformation

FP – Field Potential

GABA – Gamma-Aminobutyric Acid

GUI – Graphical User Interface

IDE – Integrated Development Environment

IPSP – Inhibitory Postsynaptic Potential

LFP – Local Field Potential

MEG – Magnetoencephalography

MEMS – Microelectromechanical Systems

MFC – Microsoft Foundation Classes

MRI - Magnetic resonance imaging

MUA – Multiunit Activity

NREM – Non-rapid-eye-movement sleep

PCA – Principal Component Analysis

PCB – Printed Circuit Board

PET - Positron Emitted Tomography

RAD – Rapid Application Development

REM - Rapid-eye-movement sleep

RMS – Root Mean Square

SD – Standard Deviation

SMR - Sensorimotor Rhythm

SNR – Signal-to-Noise Ratio

SO – Slow -Oscillation

SUA – Single Unit Activity

SWS - Slow Wave Sleep

TMS – Transcranial Magnetic Stimulation

UEA – Utah Electrode Array

UI – User Interface

2 List of figures

Figure 1: Mathematical reconstruction of the AP. Reconstruction of an AP (black curve) together with the underlying changes in Na^+ (red curve) and K^+ (yellow curve) conductance. The size and time course of AP were calculated using only the properties of membrane conductance of Na^+ and membrane conductance of K^+ measured in voltage clamp experiments. After [60]

Figure 2: Brain electrode types; the figure shows the place of recording from scalp to intracellular level (from left to right). The 2nd line shows the recorded signal. The second line from the bottom represents the size of the area from which an electrode records the sum of the signals. The last line shows the amplitude of the signal [27].

Figure 3: Different stages of NREM and REM sleep (Illustration). Note that in the new nomenclature there is no stage 4. We mentioned NREM (Stage 1 – Stage 4 in the figure) stages as N1-N3.

Figure 4: Assembled 4-mm-long active probe shaft and close-up of the probe bonded to a PCB encapsulated by two-component epoxy.

Figure 5: Manual electrode selection: Electrodes can be selected by clicking with the mouse on the electrode. Selected, unselected and non-selectable electrodes are differently color-coded.

Figure 6: The main User interface from NeuroSelect Software.

Figure 7: The selection area of the needle where user can select the preferred electrode(s).

Figure 8: The selection area of the needle with the nodes is displayed.

Figure 9: Collaboration diagram of NeuroSelect Software

Figure 10: The screenshot of the software and its window objects

Figure 11: Screenshot of Anthemion DialogBlocks

Figure 12: Closed-looped system design: (A) Electrode selection is transferred from the host computer via a controller to the microprobe. Neural signals are recorded and visualized. Based on the computed signal quality the electrodes are (re)selected. Selection is achieved via a shift register comprising flip-flops (FF): (B) Elementary cell of switch matrix, (C) single node with switch and FF.

Figure 13: Data visualization and program flow-chart of manual or semi-automatic electrode selection.

Figure 14: Spike detection - Rectangle windows of a width of 1 ms are centred around detected spikes (spikes with negative deflections in this example). Black signal is the underlying ground truth signal, after adding the real noise form the probe the signal in gray is obtained. Spikes need to be detected from this noisy signal, the underlying ground truth signals provides information on the correctness of the detection.

Figure 15: Basic steps of spike sorting. Step i) The continuous raw data is band-pass filtered, e.g. between 300 Hz and 3000 Hz. Step ii) Spikes are detected, usually using an amplitude threshold. Step iii) Relevant features of the spike shapes are extracted, thus giving a dimensionality reduction. Step iv) These features are the input of a clustering algorithm that performs the classification. Adapted from [117]

Figure 16: Implantation procedure; Animals were placed in a stereotaxic frame. Stainless-steel needle ground and reference electrodes were placed on the left and right side of the craniotomy. The probe was attached to a manual Microdrive through its mounting PCB. The EDC probe was implanted under the surveillance of a surgical microscope, so we were able to verify the depth of the implantation.

Figure 17: (A) Approximate recording position of the 4-mm long, active probe in the cortex. Close-up of eight roughly equidistant recording locations separated by approximately 300 μ m. (B) Example LFP traces from the eight recording locations. Rhythmically recurring positive (dark gray) and negative (light gray) half-waves are highlighted. (C) FFT of the LFP spectrum. (D) Example MUA traces from the eight recording locations. The original raw data were bandpass filtered between 500 and 5000 Hz.

Figure 18: State detection based on MUA. (A) Example MUA trace obtained from raw data by band-pass filtering (500 – 5000 Hz) and rectifying (arbitrary units). (B) Low-pass-filtered (30 Hz) MUA used for state detection. (C) Result of state detection based on the low-pass-filtered MUA in B. (D) Amplitude histogram of MUA envelope.

Figure 19: Up-state locked averages. (A) Up-state locked averaged LFP traces recorded from the eight locations (see close-up in Figure 17A). Amplitude inversion between contacts 2 and 3 corresponding to an approximate recording depth of 600 μ m. (B) Up-state locked averaged MUA traces. Maximal amplitude on contacts 4 – 5 corresponding to an approximate recording depth of 900 – 1200 μ m. Light shading indicates downstate; dark shading indicates up-state.

Figure 20: Average time-frequency maps of up-state locked epochs on selected recording channels 1, 3, 5, and 7 separated by approximately 600 μ m. See close-up in Figure 17A for distribution of recording channels (1 – 7) along the probe shaft. Increased (light colors) oscillatory activity in the gamma range (30 – 80 Hz) during up-state and decreased (dark colors) spectral activity during down-state in all layers.

Figure 21: (A) Representative SUA traces. (B) Isolated clusters of three units from A. (C) Raster plots of the three isolated units in B. (D) Mean spike waveforms with SD of the three isolated units in B along the eight recording channels (Figure 17A). (E) Autocorrelogram of unit 2 firing. Inset: burst firing of unit 2. (F) Autocorrelogram of unit 2 firing with longer time scale. (*) marks spindle modulation and (**) marks SO modulation of unit firing. (G) Autocorrelogram of unit 1 firing. (H) Cross-correlogram of unit 1 and unit 2 firing. (***) marks SO modulation in the cross-correlogram.

Figure 22: Phase histograms of three representative unit firings related to the phase of SO. Phase bins are represented on the horizontal axis and normalized firing rates are represented on the vertical axis. Light bars indicate down-state; dark bars indicate up-state. In all three cases, unit firing mostly occurs during up-state, while during down-state only minor unit activity is observed

3 List of tables

Table 1 Main functions of NeuroSelect software

Table 2 data structures with brief descriptions

4 Abstract

Despite the rapid advancement of brain imaging techniques offering both high spatial and temporal resolution, recording the electrical activity of the brain with electrophysiological tools is still one of the most widely used methods to investigate the complex spatiotemporal activity patterns of neuronal circuits. Over the past few decades, single-wire electrodes used for *in vivo* extracellular recording of action potentials (AP) evolved into multielectrode arrays comprising over more than a thousand recording sites [5, 6, 13, 15, 19, 24, 25, 31, 37, 38, 46, 72, 74, 76, 79, 83, 88, 91, 109, 122, 123, 132, 147, 148, 149]. With such a high number of recording sites neuroscientists are able to monitor the activity of hundreds of neurons simultaneously both in anesthetized and in freely moving animals [6, 68, 103, 142], which is fundamental for the understanding of complex neuronal computations and higher-order cognitive functions, such as learning, memory or language [18]. In addition, the reliability and performance of current invasive brain-machine interfaces, aimed to help paralyzed patients to communicate and/or interact with the outside world, significantly depends on the simultaneous recording of the activity of a high number of stable single units [59, 102, 103].

Currently, tetrodes (four closely spaced recording sites) and silicon polytodes (silicon-based multichannel electrode arrays realized using microelectromechanical systems (MEMS) technologies) are the main workhorses of neuroscience laboratories performing extracellular electrophysiological experiments [6, 13, 15, 31, 83, 92, 101, 130]. Despite the advantage of multiple recording sites, usually these devices need to be physically moved in the brain tissue after implantation to find locations with the best signal-to-noise ratio (SNR). The mechanical positioning of multielectrodes may damage a large number of axons and dendrites and increase the possibility of rupturing blood vessels, which in turn can alter the recorded neuronal activity [154]. Furthermore, recording from multiple brain regions (e.g. investigating the thalamocortical network) may need multiple penetrations from several recording probes, which further increases the severity of brain damage.

This thesis presents the *in-vivo* validation of an advanced implantable neural probe, i.e., an interface for recording of local field potentials (LFP) and multiple- and / or single-unit neural activity in the brain. It features a significantly increased number of electrodes compared to previous devices, which was achieved by the application of microsystem fabrication technologies and the integration of Complementary Metal-Oxide Semiconductor (CMOS) microelectronic circuitry. The concept of electronic depth control (EDC) enables the electronic selection of individual recording sites from high-density, silicon-based multielectrode arrays with the aid of a dedicated control software [100, 129, 130, 140]. With the recently developed CMOS-based EDC microprobes it is possible to record from a brain region and to fine-tune the

recording position according to the experimental needs without the physical movement of the probe.

The focus of this dissertation is to investigate and implement the configuration, recording, acquisition and basic data analysis infrastructure and evaluate the electrophysiological performance of EDC silicon probes. This brain-implantable probe implements a dynamically reconfigurable voltage-recording device, coordinating large numbers of electronically switchable recording sites. The results show the potential of the EDC devices to record good-quality local field potentials, and single- and multiple-unit activities in cortical regions during pharmacologically induced cortical slow oscillation (SO) in animal models.

5 Introduction

5.1 Preface

At the end of the secondary school I started to think about what is the most important subject to me in the school and which university would be the best to extend my knowledge? Well, the former was easy: biology. Every part of the living nature is very interesting, from plants to animals, from cells to mammals. I always wanted to know more and more about the mechanisms of life, how the human's systems work, like blood circulation, digestion, hormonal system and nervous system.

I had another interest that time which started to fill my spare time, called information technology. So, my main problem was that how is it possible to combine my favorite subject with my hobby? The answer was the Faculty of Information Technology and Bionics of Pázmány Péter Catholic University. I was very pleased to be admitted to the university and be part of a new community. There were some lectures after the very hard mathematics that enchanted me like neurobiology, electrophysiology or neural prostheses. The university was in a good relationship with some academic institutes and was actively supported almost every scientific work with a help of a scientific advisor. I had a huge opportunity when I was a chance to work at the Institute for Psychology of the Hungarian Academy of Sciences as a scientific student under the supervision of György Karmos and István Ulbert.

The first project I joined was the development of time frequency analysis based software for detailed examination of neural signals. At that time, I felt first the profit of the multidisciplinary approach of electrophysiology. But that was just the beginning, later I had a chance to meet and use cutting edge technologies in the field of neural probes implantation and recording techniques.

Later on, I had the opportunity to work in a project in collaboration with European partners. That time I had a great chance to work at the University of Freiburg, IMTEK, Germany for a few months to participate in a software related study, namely to investigate and implement a control software for a new type of intracortical electrode. That inspired me to continue the work with that specific electrode and associated software through in vivo experiments based on our existing result with other type of electrodes in order to validate the new device and concept.

5.2 Recent applications of neural devices

Neuroscience is a fascinating research field dealing with the complex nervous systems of animals and humans. During the last decades, remarkable progress has been achieved in explaining how the brain processes and stores information. Most of the neuroscientific researches can only be performed by using any technical devices, like brain imaging technique, optogenetics or even electrophysiological devices. Nevertheless, the goal is clear in every case, namely to interface single neurons and neuron ensembles at their different physical domains. Over the past years, the development of neural devices which were applied in humans in the one hand, have led to increasingly effective treatments and to more precise scientific results, based on neuromodulation through electrical or magnetic stimulation for several neural diseases. Among many examples, one of the most successful applications of neuromodulation is deep brain stimulation, which reduces the symptoms of different diseases, like Parkinson [93, 146] or Tourette syndrome [146], not to mention epilepsy [73] and severe depression [146]. On the other hand, some technical devices support the neural restoration of a lost function with an interface to the nervous system, called neural prosthesis. These devices have been developed to restore different sensing disorders, like hearing with cochlear implant, just to mention the best-known one.

Another interesting application of neural prosthesis is brain machine interfaces (BMI). The fundamentals of BMI are to record neural signals and transform it to a communication form or movement, which helps to keep the patient in contact with the outer world or to be closer to a normal human life. The neural activity can be recorded non-invasively along the scalp using electroencephalogram (EEG). This type of BMI can be useful when a patient suffering from locked-in syndrome (e.g. Amyotrophic Lateral Sclerosis) wants to write a letter on a computer. There are several methods to apply event related potentials (ERP) for BMI connection. Semantic anomaly (N400), P300 and contingent negative variation (CNV) are the mostly used ERPs [151]. The sensorimotor rhythm (SMR) is another brain wave rhythm, which is used for BMI. During motor imagery, the deliberate modification of the SMR amplitude can be used to control external applications [102]. However, with these non-invasive methods, the size of the recording area is relatively big which represents an averaged activity of huge number of neurons, resulting in inaccurate and slow control of several activities.

In contrast to non-invasive methods, the electrode sites can be implanted invasively into specific brain regions providing a better spatial and temporal resolution. Implanted BMI using microelectrode arrays in humans have allowed patients to move an artificial limb, i.e., a robotic arm [22, 102, 128]. Because the motor movements are represented in a distributed, highly redundant way in several cortical and subcortical areas, the extraction of different motor-control

parameters can be available with this technology. The question is how many neurons are enough to record for modelling a function (e.g. movement) and where is the location exactly from where we can record the appropriate neural activity and finally, how much the recording will be stable over time?

5.3 Brain stimulation and neural activity recording

In view of the abovementioned technologies, stimulating the brain or recording the activity of the complex nervous system is of supreme importance for neuroscience and clinical applications as well. Communication between neurons is based on electrical and chemical signals, which can be directly recorded or stimulated by neural interfaces. Currently, recording brain electric activity is the best-established interface to the nervous system. Different types of electrodes with different degrees of invasiveness and resulting spatial resolution can be used for this purpose.

Based on recent technologies, there are two possibilities for interfacing the cerebral nervous system: directly or indirectly. Direct and indirect methods can be additionally classified with respect to the interfacing physical domain. Direct interfacing can be a recording or a stimulating technique. The intracerebral interfaces dealt with in this dissertation belong to the direct recording of the cerebral nervous system. The indirect interfaces and direct stimulation of the brain is not part of the thesis even though at least as exciting fields as direct recording of brain electrical activity.

6 Cortical neural circuitry

The first part of this chapter gives an outline of the fundamentals of neurophysiology from the neuroanatomy of the brain to mechanical properties of the brain tissue and the micromotions of the brain. In addition, it gives an outline about the generation and propagation of AP. Then, in the second part of the chapter I will present recent brain electrical activity recording techniques and generation of EEG signal related to the topic of this dissertation.

6.1 Neuroanatomy of the brain

The cognitive functions of the brain are localized primarily in the cerebral cortex. The cerebral cortex is the outer layer of the brain tissue. Among others it plays a major role in consciousness, attention, language, awareness, thought and memory [70]. The nervous system has two classes of cells: nerve cells which are electrically active and glial cells, which are inactive cells. Nerve cells are the main signaling units of the nervous system, they have dedicated, morphologically defined regions with distinct role in the generation of signals and the communication of signals between neurons. These are the cell body, dendrites, the axon and the presynaptic terminals. The electrically inactive glial cells surround the cell bodies, axons and dendrites of neurons. As far as is known they are not directly involved in information processing, nevertheless they support neurons in different ways, such as producing myelin used to insulate neurons or promoting efficient signaling between neurons by taking up chemical transmitters released by neurons [70].

The cell body, or so called soma of the neuron is the metabolic center of the cell, it contains the nucleus, which is the production site of most of the neuronal proteins. The soma in general takes place between several short dendrites and a long, tubular axon. Dendrites usually branch-out in tree-like fashion and they are responsible to receive signals from other nerve cells. In contrast, the axon extends away from the cell body and at the axonal end the output of the neuron is synaptically connected to the neighboring neuron. Most axons of the central nervous system are very thin: 0,2 – 20 μm in diameter.

Rats, applied as animal model for in-vivo experiments in this dissertation, have about 21 million neurons in the neocortex [78]. In contrast, humans have impressive average numbers of neocortical neurons: 19 billion in female brains and 23 billion in male brains [111]. Each of these neurons forms thousands of connections with other neurons, building huge neural networks [70]. Despite the big difference in case of number of neurons, the neurons average

densities in rat and humans are quite similar with about 55,000 and 40,000 neurons/mm³, respectively, depending strongly on the neocortex layer and area [1, 82, 118].

Neurons are also commonly classified into three different types by their functions: sensory, motor, and interneuron. Sensory neurons are responsible for transporting information from the peripheral region of the body into the nervous system for the purpose of both perception and motor coordination. Motor neurons carry commands from the brain or spinal cord to muscles and follicles. Interneurons are the largest class, consisting of all nerve cells that are not classified as sensory or motor types. Interneurons are divided into two subclasses. Relay or projection interneurons have long axons and transport signals over significant distances, from one brain region to another. On the other hand, local interneurons have shorter axons and process information locally [70].

The rat's neocortex is about 2 mm thick; the top layer of the cerebral hemispheres is slightly thicker in humans with values between 2 and 4mm and made up of six layers with a vertical column structure of neural cells in mammals [1, 61, 96, 114, 127]. While the neocortex is smooth in rats and some other small mammals, it has sulci and gyri in primates and several other mammals. The mammalian brain is intensely folded to increase the area of the cortex and arranged in six layers with a vertical column structure of neuronal cells, called cortical columns. These cortical columns encode similar features. In case of humans, they have a diameter of 300 - 600 μm with about 10^5 neurons. Each cortical column is formed by minicolumns bound together by short-range horizontal connections, consists of microcolumns with a diameter between 40 and 60 μm and about 80-100 neurons which form microcircuits [84, 96]. There is a variety of other brain structures which were not relevant in this dissertation. For further study of neuroanatomy, related literature may be consulted [70, 116].

6.2 Mechanical properties of brain tissue

Brain tissue is a structurally and mechanically complex material with a highly nonlinear, strain-rate sensitive viscoelastic behavior [10]. It consists of gray and white matter with a Young's modulus of $E = 66.7 \text{ kPa}$ and a Poisson's ratio of $\nu = 0.499$, i.e., it is nearly incompressible [144]. Young modulus is a substance specific constant, which gives information about the stiffness of the substance. The brain is surrounded by the meninges. The subarachnoid space lies between the arachnoid and the pia mater, which, together with the dura mater, form the three meningeal layers that cover the brain. Within the subarachnoid space, fluid flows down the spinal canal and also upward over the convexity of the brain. The main function of meningeal layers is the mechanical protection of the brain against the skull particularly during head shocks. The major brain supplying arteries flow through the subarachnoid space where they give rise to branches that penetrate the substance of the hemispheres. The dura mater, which is the outermost

layer of meninges, is attached to the inner surface of the skull. It is a tough and fibrous membrane with a thickness of 0.3 - 0.8mm in humans. The dura mater has the highest Young's modulus of meninges with $E = 31.5\text{MPa}$ [155]. The middle layer of the meninges is called arachnoid because of spiderlike processes and is attached to the dura mater. The innermost layer of the meninges is called pia mater that closely overlies the surface of the brain. The pia mater has the lowest Young's modulus of meninges with $E = 11.5\text{MPa}$, mainly because it consists of only three cell layers.

6.3 Brain micromotions

The micromotions of the brain can be originate from vital physiological functions and head movements [44]. The intracranial pressure is influenced by physiological functions, i.e., respiratory and beating of the heart. In case of anesthetized rats with performed craniotomy, resulting pulsatile surface micromotions of the brain was observed to be in the order of 10 - 30 μm due to pressure changes during breathing and 2 - 4 μm due to cardiac pulsation [44]. However, when the skull is closed, then the pulsation is reduced. Lateral motions also occur in the brain due to head accelerations, which mainly causes rotational brain movements.

6.4 Action potential generation

In this chapter the reconstruction of AP is derived based on Hodgkin and Huxley's equation. Neurons can carry signals over long distances because of their ability to generate AP, so the communication of neurons is based on APs, so-called spikes, which are regenerative electrical signals whose amplitudes don't attenuate as they move down the axons. The Hodgkin - Huxley equation is a mathematical model that describes the mechanism of an AP of a neuron, i.e., how APs are initiated and propagated. From their experiments, they could construct a detailed mathematical model of the sodium (Na^+) and potassium (K^+) conductance changes. The goal was to determine whether these conductance changes alone are sufficient to produce an AP. Their mathematical reconstruction showed that they could in fact generate the form and time course of the AP with high accuracy (Figure 1). The voltage of a neuron membrane is influenced by the signals of the adjacent neurons contacted via synapses and dendrites. Chemical synapses are based on the secretion of inhibitory and excitatory neurotransmitters in the presynaptic neuron. These neurotransmitters diffuse across the synaptic cleft with a width of 20 nm and bind to the receptor site on the postsynaptic membrane [57]. Synaptic events change the membrane potentials in the postsynaptic dendrites and somata, called postsynaptic potentials. Depending on the function of the synapse, the potential is called excitatory postsynaptic

potential (EPSP) or inhibitory postsynaptic potential (IPSP). When a threshold input potential of -55mV is exceeded, voltage-gated Na^+ channels of the neurons open. The Hodgkin – Huxley model showed that the selected increase in Na^+ conductance is responsible for AP initiation. The increase in Na^+ conductance causes Na^+ to enter the neuron, thus depolarizing the membrane potential, which approaches the equilibrium potential of Na^+ (55 mV). The rate of depolarization subsequently falls both because the electrochemical driving force on Na^+ decreases and because the Na^+ conductance inactivates. At the same time, depolarization slowly activates the voltage-dependent K^+ conductance, causing K^+ to leave the cell and repolarizing the membrane potential toward the equilibrium potential of K^+ (-90 mV). Because the K^+ conductance becomes temporarily higher and Na^+ conductance becomes lower than they are in the resting condition, the membrane potential actually becomes briefly more negative than the normal resting potential. The hyperpolarization of the membrane potential causes the voltage-dependent K^+ conductance (and any Na^+ conductance not inactivated) to turn off, allowing the membrane potential to return to its resting level. Under consumption of ATP, the energy source of the cells, the sodium and potassium ions are finally transported back into their original media. Nevertheless, the above-mentioned transport back mechanism does not play a critical role in the generation of the next AP by itself, because the ions, exchanged under an AP, cover only a small fraction of the accumulated concentration difference. It follows that, a single neuron can emit several APs without the long-term recovery activities of the pumps.

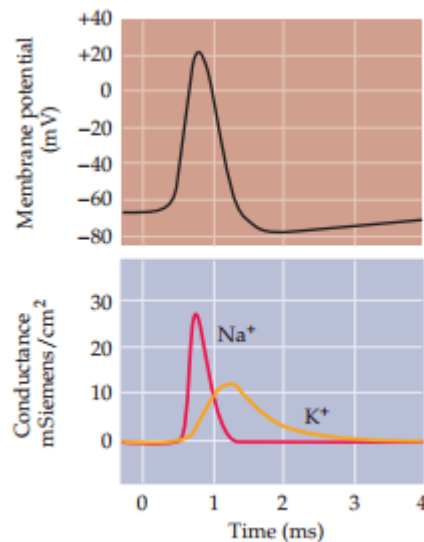


Figure 1: Mathematical reconstruction of the AP. Reconstruction of an AP (black curve) together with the underlying changes in Na^+ (red curve) and K^+ (yellow curve) conductance. The size and time course of AP were calculated using only the properties of membrane conductance of Na^+ and membrane conductance of K^+ measured in voltage clamp experiments. After [60]

6.5 Propagation of the action potential

Once an AP is generated at one point of the neuron, how does it propagate to the synaptic terminal? The electrical current depolarizes the adjacent region of the axon membrane. As the charge moves to the adjacent region of the axon, it will depolarize too. If it will depolarize efficiently, voltage dependent Na^+ channels in the adjacent regions will be opened and a new AP will be generated, so AP regenerates itself while the refractory time prevents the AP from traveling back along the axon. In fact, the propagation velocity of the APs in nerves can vary from less than 1 meter per second to more than 100 meters per second. In case of myelinated nerves, the propagation of AP is different. Myelin turns off all the voltage-dependent Na^+ channels, so the AP can not propagate actively. Rather, the potential change produced by the AP at one node (called node of Ranvier) spreads in the internodal region along the axon passively, allowing a saltatory propagation of the AP, resulting increased velocity. Although, myelin insulates the membrane though, in the nodes of Ranvier have the greatest density of the voltage dependent Na^+ channels and have also the greatest active currents, which contribute to the extracellular action potentials (EAP), such as the capacitive currents [45]. During the initiation of an AP, the soma can be depolarized as well. This depolarization can spread towards the dendritic tree where there are voltage gated Na^+ channels and it can result in the propagation of dendritic AP, called backpropagation and believed to be responsible for synaptic plasticity [7, 16, 53].

6.6 Non-invasive recording methods

The analysis of bioelectrical signals of the brain is a non-invasive or invasive method to investigate cerebration. EEG is a method that measures and records the oscillations of brain electric potentials recorded from special sensors, called electrodes, attached to the scalp and hooked by wires to a computer. The electroencephalography is also a clinical examination.

The recorded brain electrical signals are transmitted to several amplifiers, filters, and finally displayed on paper chart or computer monitor. EEG technique is discovered by Hans Berger in 1924. He described the alpha wave, which is measured from occipital areas of the brain during wakefulness when the subject's eyes were closed. He also observed that alpha waves disappeared when the patient's eyes were opened again [8]. Perhaps Berger's discovery was a huge step forward in electrophysiology, yet that time his findings did not gain widespread acceptance in the scientific community but by 1937 he gained the approval of Lord Adrian, who, as a psychologist, took a particular interest in alpha waves [71].

Recently EEG and magnetoencephalography (MEG) are the most popular non-invasive technologies with acceptable temporal resolution to follow the fast-dynamic changes in the brain. Otherwise, the spatial resolutions of EEG and MEG are low, relative to other brain imaging techniques like magnetic resonance imaging (MRI), computer tomography (CT) and positron emitted tomography (PET). Every electrode of the scalp EEG records electric potentials from a relatively large brain area, which are generated in tissue with up to one billion neurons in the cortical layer. [108]

Therefore, scalp EEG activities are showing the summation of the synchronous activity of thousands or millions of neurons with similar spatial orientation. Ions of cells with different spatial orientation do not line up and create waves to be detected. One good example is that the Pyramidal neurons of the cortex are known as the most responsible cell type in the brain which activities are present in the EEG signal, mostly because they are fire together and well-aligned. It is more difficult to detect neural activity from deep sources than currents closer to the skull, because voltage fields fall off with the square of distance [77].

6.7 Invasive recording methods

The electrodes of electrocorticogram (ECoG) record the same signal as in EEG, with closer proximity to the brain. ECoG electrodes are surgically placed on the surface of the cortex. In addition, with the elimination of the insulating part of the skull and dura, recording signals result in greater signal amplitude, wider detectable frequency range, and better topographical resolution [17].

If we are moving towards to a better space resolution, intracortical methods can be a good solution to record LFP and neuronal APs. These intracortical methods are the most invasive, since they record electrical activity from electrodes implanted in the brain (Figure 2).

Thus, compared with traditional EEG, ECoG and intracortical recordings also provide wider frequency range, higher topographical resolution and better signal quality. However, both methods are invasive, and tissue damage, infection, and long-term recording instability can make more difficult their usefulness [59, 152].

Basically, two main groups of invasive electrophysiological recording techniques are known. These are the extracellular and intracellular recording techniques. In the next paragraphs these techniques will be presented in order to better understand later the goals of the EDC probes.

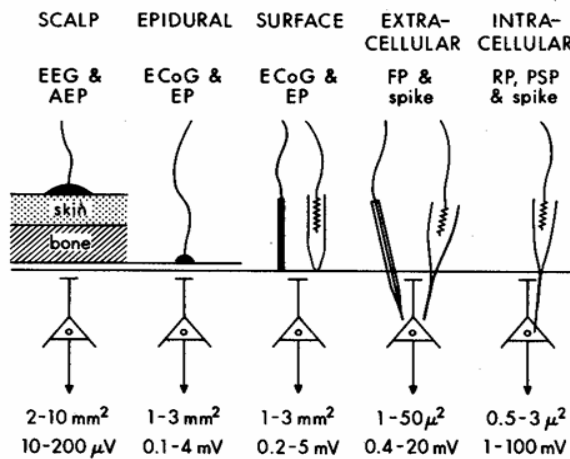


Figure 2: Brain electrode types; the figure shows the place of recording from scalp to intracellular level (from left to right). The 2nd line shows the recorded signal. The second line from the bottom represents the size of the area from which an electrode records the sum of the signals. The last line shows the amplitude of the signal [27].

6.7.1 Extracellular recording techniques

As the name of the group suggests, the extracellular recordings take place in the extracellular space. These techniques serve to record many neurons' activity (population activity). This technique measures field potentials which is the sum of the transmembrane activities. We can measure the AP activity of cells, which is single or multiunit activity. If we are very close to a cell, then we can measure its single unit activity, which is the AP of the neuron [18, 120].

The type of the measuring electrode can be micropipette, wire electrode with one contact, multi wire electrode (tetrode, multielectrode) or silicon based multielectrode.

With these types of electrode, we cannot detect APs obviously (Figure 2). The voltage at the electrode conductor depends on the strength of the field and thus the proximity of the electrode to the field source. This capacitive source is typically small, on the order of few hundred microvolts, meaning that the recording system needs to be very sensitive, and the electrical noise poses a significant challenge, not to mention the high number of neurons around the electrode in the extracellular space. High electrode impedance can also cause problems for recording APs. [120].

6.7.2 Intracellular recording techniques

Intracellular recordings, as their name reflects to it, are measuring from the cell. For that, somehow we have to penetrate into the cell. In this case, single neuronal activity, or in

some cases a few neurons' activity can be measure in parallel. We measure directly the synaptic and membrane potential activity of the cell. In addition, we can measure the ion channels and membrane currents, even only one ion channels activity. And we can add chemical materials under the measurement [50, 120].

The used electrode type is often micropipette; the MEMS based electrodes are very rare today.

6.8 Origins of the brain electrical signal

Although, we discussed above the available technologies for measuring brain electrical activities, we have not mentioned yet, what do we record when we use these methods? Because in this dissertation we are focusing on intracranial brain electric activity recording techniques, in this chapter, I try to summarize the origins of the brain electrical signal in short.

The EEG gives an appropriate window on the mind, revealing synaptic activities of neural cells that are in good relations with brain states. Most of the EEG signals are generated in the cerebral cortex, believed liable for our behavior, individual thoughts and emotions. The characterization and quantification of the population activity of neurons can do with the help of field potentials. The synchronously active neurons' membrane currents flow through the extracellular space and the potential changes are measurable with a proper electrode. The EEG is one of the most commonly analyzed field potential. Potential waves of different frequencies originated from the cerebral cortex can be registered with electrodes placed on the scalp or the surface of the cortex. The some 10 μV macropotential waves are primarily generated by the slow potential changes of dendrites and somas. Under the synaptic activity, positively charged ions, that are moving to the inner part of the cell are generating negative current (sink) and, as a result of charge conservation, positive ions flow out from the other side of the cell, which process is called positive current (source).. These two currents together create a dipole and the circuit closes through the extracellular space. The main sources of the EEG signal are the slow synaptic potential changes (EPSPs and IPSPs) and non-synaptic currents such as post hiperpolarizatons evoked by bursts. APs do not play an important role in the genesis of EEG, since they summed difficultly because of their short duration ($< 2\text{ms}$) and only small membrane areas are affected during their formation. The extracellular space of the neural tissue does not conduct high frequency electrical waves well, which prevents the cumulation of high frequency signals in space. The geometry of neurons is important in the genesis of the EEG, as well. The cell with concentrically placed dendrites does not generate macropotential change, because dipoles in different directions cancel each other. The places from where we can registrate the

best field potentials are the ones which contains long-drawn shaped cells, like in the cortex or hippocampus, where big pyramidal cells have this kind of morphology. The potentials of individual cells have very small amplitudes, the requirements of their registration are on one hand the superposition in space and time of numerous cells' potentials and on the other hand the appropriate degree of amplification. Synchronization means the fluctuation of membrane potentials in the adjacent cells collated in time. Conversely, if the neurons' electrical activities are not coordinated in time, then signals of individual neurons mostly cancel each other out, which mechanism is called desynchronization. At this time, small amplitude and high frequency waves are dominant in the EEG signal [105, 108]. The waves are different in every state of vigilance. The typical patterns of sleep will be discussed later.

7 Properties of sleep

In this chapter I will summarize the main functions of sleep and sleep stages, focus on the deepest sleep stage, walking around the properties and generation of this stage.

7.1 Sleep – in general

Although at first look it is obvious what sleep is, it remains difficult to define it or simply put it into definitive terms. As the American Sleep Association defines, sleep in general is:

„a normal active state of all living creatures in which the mind and body are less responsive. It is believed that sleep is a restorative process.“

Or in other words which is more specific:

„The definition of ‘sleep’ is that it’s a naturally recurring state of mind that’s characterized by altered consciousness, the inhibition of almost all voluntary muscles, generally inhibited sensory activity, and a marked reduction in our interactions with our surroundings.“

We spend about a third of our lives in unconscious, unprotected and vulnerable state. Perhaps strong or important stimuli can wake up from this state; it is undoubtedly full of dangers. Nonetheless, we still cannot know why do we sleep, what happens exactly when we sleep, how much do we sleep and why do so many people have sleep problems? It must be very important, because sleep deprivation can be as painful as torment. Sleep is necessary and can be observed in most of the mammals and birds. Though there are some exceptions, sleep is associated with special EEG patterns. The behavioral properties of sleep are complex: rapid reversibility, place preference / specific position, increased arousal threshold, homeostatic regulation, and often circadian regulation [14].

Sleep research is conducted in three different directions: homeostatic -, daily rhythmic- and neural regulation. These are mostly independent research areas.

Homeostatic regulation is based on the search for sleep factors, effects of sleep deprivation and the function of sleep. Daily rhythmic regulation is about the measurement of activity and rest, alignment to the outside world and the biological clock. Neural regulation of sleep is measured by electrophysiological methods. It is examining the waking systems and sleep centers of the brain and try to explore the relationship between the alertness and EEG. In this dissertation, I only focus on the latter research area.

7.2 Sleep stages

Sleep can be divided into different stages, which follow a specific pattern in animals and humans alike, though the duration and properties of these stages may vary from species to species.

In general, sleep can be divided into two types, which are rapid-eye-movement (REM) sleep and non-rapid-eye-movement (NREM) sleep. REM sleep, often called "active sleep," on a human EEG is recognizable by its characteristic high-frequency (fast), low-amplitude (small) waves, as well as the eye movements for which it is named. During sleep, we usually go through five phases of sleep which consist of N1-N3 (N4) and paradoxical sleep states (Figure 3). In humans, during stage N1, which is light sleep, we drift in and out of sleep and can be awakened easily. Our eyes move very slowly and muscle activity slows. People awakened from stage N1 sleep often remember fragmented visual images. Many also experience sudden muscle contractions called hypnic myoclonia, often preceded by a sensation of starting to fall. These sudden movements are similar to the "jump" we make when startled. When we enter stage N2 sleep, our eye movements stop and our brain waves (fluctuations of electrical activity that can be measured by electrodes) become slower, with occasional bursts of rapid waves called sleep spindles. In stage N3, extremely slow brain waves, called delta waves begin to appear, interspersed with smaller, faster waves. By stage N4 in the old nomenclature, the brain produces delta waves almost exclusively. It is very difficult to wake someone during stages N3 and N4, which together are called deep sleep. Eye movement and muscle activity disappear. People awakened during deep sleep do not adjust immediately and often feel groggy and disoriented for several minutes after they wake up [135]. From 2008, the American Academy of Sleep Medicine (AASM) has discontinued the use of stage four (N4), such that the previous stages N3 and N4 now are combined as stage three (N3). An epoch (30 seconds of sleep) which consists of 20% or more slow-wave sleep now is considered to be stage three (N3) [67].

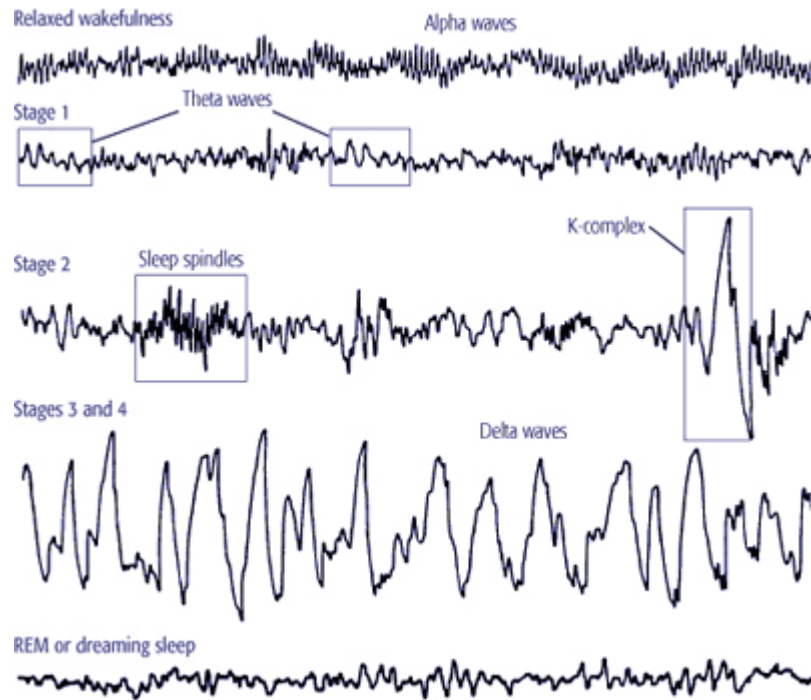


Figure 3: Different stages of NREM and REM sleep (Illustration). Note that in the new nomenclature there is no stage 4. We mentioned NREM (Stage 1 – Stage 4 in the figure) stages as N1-N3.

In all mammals and many other animals, sleep can be defined in much the same way that we define sleep for humans. However, there are some notable differences among species. When humans sleep, the entire brain is involved. On the other hand, whales and dolphins, need to maintain consciousness while they sleep so they can occasionally come to the surface to breathe. In these marine mammals, sleep occurs in only one hemisphere of their brain at a time—allowing for some degree of consciousness and vigilance to be maintained at all times. In the next chapters, only the slow wave sleep (SWS) phase of sleep is detailed.

7.3 Slow wave sleep and slow oscillations

SWS is considered the deepest phase of NREM sleep, dominant during the first half of the night. It is accompanied by maintained muscle tone, higher threshold of arousal, and high-amplitude, low-frequency (< 2Hz) waves on the EEG [133-135].

Delta waves during sleep were reported in 1937 by Blake and Gerard [12], but SO, the main characteristic electrophysiological features of deep sleep were first described in anesthetized cats by Mircea Steriade in 1993 [134]. They later detected SO in other mammals and humans, too [2], during various arousal states like anesthesia, natural sleep [34], and quiet wakefulness [115] Furthermore, Slow oscillation (SO) can be induced in slices, too [125].

In animal models, during anesthesia, the membrane potential of the cortical neurons is measurable under SO. These measurements showed that SO consist of the alternation of two states in the membrane potential of cells: an active, depolarized state, during which the membrane potential is closer to the firing threshold and neurons generate APs (also called up-state), and an inactive, hyperpolarized state, during which the membrane potential is more negative with virtually no firing (down-state) [137]. The cortical LFP recorded in cats with a laminar extracellular electrode is positive superficially during up-states that turns into negativity in deep layers. During down-states a superficial negativity and deep positivity can be detected. During up-states, fast oscillations emerge, while during down-states they disappear.

In human SWS, the alpha and beta power is increased during the surface positive half-wave (up-state) compared to the surface negative half-wave (down-state), suggesting that their basic neurophysiology may be similar to animal findings [89, 94]. While the SO in animals is limited to below 1 Hz [134], the recent AASM guidelines suggest the 0.5 - 2 Hz range for SO in humans [67].

The fine scale laminar structure of neuronal activity was analyzed in ferret slice preparations, revealing that firing during the up-state is the earliest in the infragranular layers and spread towards the superficial layers with a long ~100ms inter-laminar delay [125]. In intact animals, the up-state onset related initial firing, intracellular membrane potential and LFP changes could be detected in any layer in a probabilistic manner, with a short inter-laminar delay (~10ms), however, on average, the earliest activity was found in the infragranular layers [23, 124]. Subthreshold membrane potential fluctuations giving rise to LFPs clearly precede neuronal firing at up-state onset, thus, firing may be the consequence rather than the cause of up-state initiation [23].

Current source density analysis revealed that the low frequency (<1 Hz) components of the anesthesia induced SO in cats displayed a massive current sink in the middle layers (most probably layer III-VI), confined by two sources in superficial and deep layers, while fast oscillations (30-40 Hz) were more distributed, composed of alternating microsinks and microsources along the whole cortical depth [136]. During spontaneous and evoked SO-like events called the K-complexes, a massive up-state related sink was reported in layers II-III besides weaker ones in the deeper layers [3]. In still another cat study, the maximal sink during the up-states in natural sleep was located in the middle and deep layers [23]. In the rat primary auditory cortex, the laminar distribution of the major up-state related sink was variable [124]. On average across animals, it was located in middle and deep layers (most probably layer III-V) in natural sleep, whereas it was located in superficial layers (most probably layer II-III) under urethane anesthesia [124]. Although the cellular and synaptic/trans-membrane mechanisms of

slow waves during natural sleep are thus under intense investigation in animals, these mechanisms have not previously been studied in humans.

Up-states are proposed to be micro-wake ‘fragments’, similar to the activated state of waking [35], while down-states are considered silent states filtering stimuli to the cortex.

Other important role of SO is consolidating engrams to the facts, or in other words, memory consolidation during SWS, which effect can occur in a particular, well defined region of the brain locally [145]. The neural mechanism of memory consolidation may be probably varied. One neural mechanism is the so called synaptic homeostasis model, where those synaptic connections remain in SWS, which reached a certain weight, while synapses with lower weight will disappear. So, the consolidated synaptic connections will be stronger and more stable [145]. For strengthen connections between neural cells, the other important factor might be the reactivation of those neural cell ensembles in sleep which are in connection with the memory traces formed in awake state. Recent studies showed that SO can induce long term plasticity in the thalamocortical system [23, 137]. Another possible way for memory consolidation during sleep might be the cortico- hippocampal interaction [94].

7.4 Generators of the slow oscillation

SO can be detected in several brain structures: all neocortical areas (in all types of neurons and glia cells), thalamus (in thalamocortical and reticular neurons as well), hippocampus [95], basal ganglia [141] and in cerebellum driven by the neocortex [121].

Despite, SO is traditionally considered an oscillation generated by neocortical networks. The main arguments for its neocortical origin are that it is present in the neocortex after thalamectomy [134], but absent in the thalamus after decortications [138], and the disconnection of intracortical synaptic linkages results in the disruption of its long-range synchronization [4].

Recently, the pure neocortical origin of SO has been disputed. Crunelli and Hughes pointed out the crucial role of thalamus in the generation of SO [28]. They argue that SO in isolated cortex was not identical to those present when all connections were intact; and SO can be detected in thalamic slices if the metabotropic glutamate receptors (mGluR) of thalamocortical or reticular neurons were activated. They suggest that SO can be generated in three structures:

- cortical circuits (due to synaptic network properties),
- thalamocortical neurons (intrinsically, depending on glutamatergic input from the cortex),

- reticular neurons (intrinsically, depending on glutamatergic input from the cortex),

and the interplay of these oscillators is necessary for the full manifestation of SO. Furthermore, they mention the observation that high-frequency (150 - 300 Hz) bursts of thalamocortical neurons mediated by a low-threshold Ca^{2+} potential consequently precede the firing of cortical cells and the depth-negative peak of the LFP in the cortex. This could point to that the generation of up-states thus may be triggered by thalamic input.

Other theories for the activation of persistent sodium current that is essential for up-state initiation [87] include spontaneously occurring coincidence of mini EPSPs or the action of some neurons that have a slightly lower spiking threshold. But subthreshold membrane potential fluctuations clearly precede neuronal firing at up-state onset, thus, firing may be the consequence rather than the cause of up-state initiation [23].

Mechanisms generating and maintaining down-states are also debated. Input resistance was found to be the highest during the down-states and lowest during the early part of up-states, increasing until its end [36]. Furthermore, during down-states, inhibitory neurons are silent, too. Thus, instead of an active inhibition, the hyperpolarization is thought to be the result of disfacilitation i.e. the lack of firing of input neurons [26], or the buildup of activity-dependent potassium conductances [125] or both [58]. K^+ currents are believed to be the main factor in generating down-states since the application of Cs^+ acetate, nonspecific intracellular blocker of K^+ currents, reduces hyperpolarization up to disappearance [139]. However, it has been shown that GABA_B has an important role in terminating up-states [86]. Indeed, the observation that the onset of down-states is synchronized more precisely than the onset of up-states suggests a long-range synaptic mechanism [143].

Experiments on cats and rats anesthetized with urethane or ketamine/xylazine revealed a slow cortical activity similar to that observed during natural SWS [23, 26, 47, 48, 85, 131, 133, 134, 143]. Anesthesia-induced SO appears more regular than SWS [134, 150], and its frequency was higher with ketamine/xylazine than urethane anesthesia [131, 134] indicating that properties of SO are not fixed, but depend upon experimental conditions. Recordings from different cortical areas show a preferential origin of slow waves at specific locations [89, 143, 80, 106], suggesting regional specificity.

Ketamine-xylazine anesthesia is extensively used as a model of sleep SO. The differences between patterns of slow waves in LFP observed during SWS and anesthesia in different cortical areas were corroborated by results of intracellular recordings. However, during anesthesia the SO appears to be more rhythmic. Furthermore, during anesthesia the SO was of overall higher amplitude and the silent states were of longer duration than in SWS [23].

7.5 Reactive properties of sleep

SOs occur spontaneously during anesthesia and deep natural sleep, but they can be evoked by external stimulation, too. K-complexes can be evoked during sleep by sensory stimuli, and though the mechanisms underlying their generation are likely similar to those of the hyperpolarized phase of SO [20], they are isolated phenomena not constituting an ongoing oscillation that may distinguish them from the fully developed SO. It has been shown that sound stimuli can entrain the SO in the thalamus [43, 51], furthermore, SO can be induced by transcranial magnetic stimulation (TMS) in humans [90], and by electrical stimulation in rats [110, 145] and humans [40].

Massimini et al. showed that slow waves triggered by TMS resemble spontaneous waves in their morphology and propagation properties [90]. Every TMS pulse evoked a slow wave that started under the stimulator and spread over the scalp. Interestingly, while slow waves could be evoked in any phase of NREM sleep, either local (indicating the breakdown of connectivity during sleep) or global (an aspecific response), responses during waking were long-range and specific, with a low-amplitude, complex wave shape.

Entz et al. showed in humans that slow waves can be evoked by cortical electrical stimulation and characterized the laminar profile of evoked waves [40]. They showed that the LFP, MUA, spectrogram, and current-source density attributes of intracortical responses are similar to those measured during natural SO. Responses triggered in different vigilance states (awake, sleeping, and anesthetized) differed only in the amplitude and latency of evoked potential components derived from subdural electrodes [40].

8 Advances in electrode fabrication

In this section I will present recent brain implantable electrode technologies, including their fabrication processes and technological barriers.

8.1 From hand assembled electrodes to MEMS based probes

The scientific need for multiple-site brain electrical activity recording capability fueled the elaboration of various multisite voltage-recording microelectrode probe arrays. Different technological solutions have been reported to implement these devices depending on the user demand, brain area to explore, and experimental approach. Manual construction technologies, such as wire-based probe assembly, were used earlier to build probes and record neural signals with many sites in acute or in chronic experiments.

Although these manual technologies are considered to be outdated, there are still many laboratories using hand-assembled stereotrodes [91], tetrodes [109] [147], and other micro-wire bundle arrays [72, 79]. The reason for their continuing usage is mostly because of the convenience of their construction, their durability, and the possibility to physically reconfigure the location of the wire-based probes with respect to the brain tissue, if experimental needs require it.

In the last decades, MEMS technology became expedient enough to take the technological lead in constructing brain-implantable devices [148]. As the most commonly used carrier material of these probes is silicon (Si), they are called nowadays the silicon probes [19].

Well-known silicon probes include the Utah electrode array (UEA) [19, 9] and the Michigan probes [148, 13, 31], as well as neural probes developed at the California Institute of Technology (Caltech) [38, 39] and by the consortia of the European projects NeuroProbes [100, 123] and its extension NeuroSeeker [122]. In the next paragraphs I will summarize the main properties of the abovementioned silicon probes.

8.2 Utah Electrode Array

The UEA is a silicon-based monolithic structure designed for use as a multichannel interface to the central nervous system. The UEA consists up to 128 silicon needles in various configurations carrying a single electrode on each tip. The standard electrode lengths are between 0.5mm – 1.5mm and have a pitch of 400 μm depending on the experimental need [19]. Electrode site metal options can be made of platinum or iridium oxide. Electrodes are sputter

deposited on the needle tips while the needles themselves are isolated by parylene-C. The UEA electrode arrays are commercially available from Blackrock Microsystems (Salt Lake City, UT, USA) [11].

The probe length of the UEAs is limited by the silicon wafer thickness. Recently, the longest probe length is only 1.5 mm. Further, each probe shaft contains only one recording site and the fabrication process suffers from low production rates because of atypical batch process. The interconnection of the UEAs is made of a set of gold wires insulated with polyimide. It is bonded on the back of the array to a set of aluminum read-out pads ultrasonically. The rigidity of the metal wire bundle makes UEAs inappropriate for chronic implantation in human brain [49].

8.3 Michigan Probe

In contrast with UEA, Michigan probes comprise slender needle-like probe shafts consisting of multiple planar electrodes on the surface of the shaft. Depending on the experimental application, the standard array site layouts can be linear, edge, tetrode, polytrode and multi shank. The standard Michigan probes have a thickness of 15 μm or 50 μm which varies by design, length of 2, 3, 4, 5, 6, 10 or 15 mm, and width of 123 - 145 μm at the base narrowing to 125 - 19 μm at the tip [37, 69]. The probes comprise Iridium (standard), Platinum (custom) or Gold (custom) electrodes, gold bonding pads and polysilicon interconnecting lines. The recording sites have sizes between 25 and 1250 μm^2 with spacings in the range from 20 to 200 μm [37]. Probes with four [113], eight [75, 113, 153], sixteen [18, 31] and thirtytwo [69] electrodes per shaft have been fabricated, reaching up to 256 channel count with 3D matrix array or 2D Buzsaki probe with 32 recording sites on 8 shanks. The increased number of electrodes has been achieved by reducing the width and space of the interconnecting lines between the electrodes and connector part down to 1.5 μm defined by the lithography step. However, the increased number of electrodes results in large connector bases and printed circuit board (PCB). The Michigan probes are commercially available in various configurations with single and multiple shafts from NeuroNexus (Ann Arbor, MI, USA) [99].

Michigan probes have been successfully used in several neuroscience applications since decades, but they also suffer from some disadvantages, related to probe thickness and durability, in one hand. The typical probe thickness of Michigan probe is 15 μm . These probes when inserted through the meninges of the brain needed special insertion tools. Mechanical weakness of the probes may result in probe fissures and fractures and may cause severe brain tissue damage during insertion. On the other hand, the fabrication process for Michigan probes

typically involved anisotropic etching with ethylene diamine pyrocatechol and using boron etch stop technique, which is incompatible with on-shaft integration of CMOS circuitry.

8.4 NeuroProbes and Caltech Probes

In case of NeuroProbes [54, 56] and Caltech probes [38, 39], in contrast to wet etching with boron etch stop, probes were structured by dry etching of silicon wafers, i.e., by deep reactive ion etching (DRIE) [42]. Their fabrication varies in front DRIE of thin wafers [39], double-sided DRIE of standard [54] and silicon- on- insulator wafers [107, 38] and front DRIE and rear side wafer grinding [56]. This results in powerful fabrication processes for batch processing with high production and adequate robustness of the probe shafts needed for insertion [54]. The probes thicknesses are in the range of 20 and 100 μm . The layout of the electrode contacts along the probe shafts results in a trade-off between resolution and maximum extension of the volume to be covered by the probe array. The maximum achievable number of electrode contacts per shaft is defined by geometrical limitations, i.e., optimize the width of the shaft considering minimized tissue damage and lithography defined spacing and width of the interconnecting lines. 5 μm [55], 1.5 μm [13], 1 μm [107] and 0.29 μm [38] electrode line widths and spacings were realized. Thanks to the e-beam lithography, the finest resolution is allowing 64 electrodes along a 1.5 mm-long shaft.

8.5 Mechanical adjustment of electrode position

It is a common practice, when the experimenters need to adjust the position of the passive microelectrodes for better signal quality or population activity, which is mostly achieved by mechanical adjustment of the insertion depth of the wire electrodes using micromanipulators and motorized microdrives [126, 41, 21]. Although, the manual replacement of the probe thereby depends on the experimenter's intuition and subjective assessment with the aid of oscilloscopes and loudspeakers in order to find high quality signals in neural recording [21, 98]. Furthermore, advanced experience is required to find and isolate single-unit activity (SUA) from background activity. With the integration of thermal microactuators, this mechanical depth control was adapted to microelectrode arrays [97], allowing the displacement of three polysilicon probe shafts of up to 5mm at a resolution of 8.8 μm . However, electrode positions cannot be optimized individually within the neural tissue, because all electrodes along the probe shaft are translated in synchrony. One of the major drawbacks using thermal microactuators is that because of micromotions of the brain it cannot be applied to compensate for position shifts of the probe relative to the neural tissue in chronic implantation [97, 21]. In addition, the

probability of inflammation, reactive gliosis and apoptosis of brain tissue is increased by the mechanical movement of the probe, which can end with the degradation of the recorded signals [31].

9 Objectives

Recent applications of neural devices and the corresponding electrophysiological background have been introduced in the previous chapters. The difficulties that ensued from the micromotions of the brain and the need for high-density electrode arrays for intracortical recording are clearly indicated a solution which is capable to record stable and good quality neural signal. Current electrode arrays are not able to satisfy this need in long term, because of their limited number of electrodes and their manual positioning capability if signal quality is getting worse, which can cause inflammation or brain tissue injury.

In addition, properties of sleep and mainly SO have been also presented. The characteristics of SO are well defined based on animal models.

The main objective of this dissertation is the in-vivo validation of a novel, implantable intracortical interface comprising high-density electrode array based on CMOS-integrated MEMS technologies. It is capable to record single neural activity with high resolution and no need to manually adjust electrode positions due to integrated EDC technology. The thesis details the setup, experimental in-vivo studies and corresponding data analysis through the properties of SO, based on previous research results, successfully demonstrating the concept of EDC. To understand the above need, recent spike sorting algorithms and time- frequency analysis methods which related to our results are also investigated.

Furthermore, probe system development, including software for real-time data acquisition and visualization is also an important part of the dissertation.

10 Electronic depth control concept

There is a strong demand from the scientific point of view to record from as many locations from the brain as possible to better understand the large-scale machinery of neural networks, facilitate reproducibility and to characterize interindividual differences. To fulfill the experimental necessities of the mass neural recording demand, usually a limited number (16–32) of recording sites are implemented on a single silicon probe shaft and the probe is physically moved with respect to the brain tissue in order to explore gradually more and more brain areas. Of course, this approach poses the risk of probe breakage, especially in the case of the rigid silicon carrier and, most important, tissue damage due to frictional forces and bleeding from the rupture of blood vessels [46]. To overcome the fragility and tissue damage problem and establish large numbers of neuronal recording sites in a relatively wide brain area, we have developed EDC devices using MEMS or CMOS technology [100, 122, 123, 129, 130]. These devices resemble a regular silicon probe in shape; however, instead of having only a limited number of recording sites, they have 188 recording contacts occupying a considerably larger proportion of the area of their 4-mm long shaft. Of the 188 possible contacts, eight sites can be electronically selected and routed out to an external amplifier to record neuronal activity simultaneously from the eight sites. The selected sites can be rapidly reconfigured, allowing the experimenter to record from widespread brain areas without physically moving the device [130].

In addition, it is important to mention that other types of EDC electrodes are under development, like two-dimensional (2D) arrays. 2D probes were realized using a commercial 0.5- μm CMOS process for the EDC circuits combined with post-CMOS micromachining to pattern the comb-like probes and the corresponding electrode metallization. A dedicated CMOS integrated front-end circuit was developed for pre-amplification and multiplexing of the neural signals recorded using these probes [140]. The in-vivo validation of 2D probe is in progress, however the opportunities in this type of electrodes are as exciting as it was in the subject of this dissertation, not to mention the inter-regional relationships between different brain areas like thalamocortical pathway is.

10.1 Gliosis and biocompatibility

Biocompatibility and long term viability are important questions for chronic implantable devices. We examined the NeuroProbes silicon microprobes earlier and our data showed that these types of probes are highly biocompatible. Neural loss around the probes was evident within 100 μm , but it was considerably reduced with time, with neuronal densities returning up

to 90% of control levels at 2-4 weeks after implantation. In addition, a moderate gliosis occurred around the probes in cases of minor or no bleeding, but a dense glial scar did not develop. We coated the silicon probes with different types of bioactive molecules, but we did not find any significant differences in our results in terms of tissue reactions, except when we used dexamethasone (DexM), which showed minor effects on neuronal tissue survival as compared to native silicon probes.

In summary, our study suggested to avoid blood vessel disruption during implantation, which could be the most effective way in preserving neuronal density around the probes [V].

10.2 Electronic depth control probe

The 180- μm -wide, 80- μm -thick, 4-mm-long, 19° tip angle penetrating shaft of the EDC device was realized using DRIE of silicon. The shaft is populated with 188 recording sites in two columns with an equal horizontal and vertical center pitch of 40 μm . The 20- μm -diameter recording sites were plated with Pt, measuring about 1 M Ω impedance at 1 kHz. Each recording site can be connected internally to one of the eight output lines of the probe, and these output lines can be connected in turn to an outside amplifier [130]. The connection matrix, switching electronics, control, and input and output lines were integrated on the shaft of the probe, implemented by the 0.6 μm CMOS process XC06 (X-FAB Semiconductor Foundries AG, Erfurt, Germany). Post-CMOS fabrication, including the recording site, metallization and DRIE of the CMOS wafer for electrode shaft shaping were carried out at IMTEK (University of Freiburg, Freiburg, Germany). The input and output lines of the probe were wire bonded to a PCB and encapsulated with technical grade epoxy (Figure 4). The EDC device is reconfigurable using a field-programmable gate array (FPGA)-based controller (XC3S200, XILINX Spartan) on a separate PCB, through the parallel port of a personal computer. The graphical user interface (GUI, NeuroSelect) software made it possible to visualize electrode selection and reselect different configurations according to the experimental situation. The settling time after configuration reselection depended on the DC value mismatch between the electrodes switched and the time constant of the amplifier used. The switching transient itself lasted about 10– 100 ms.

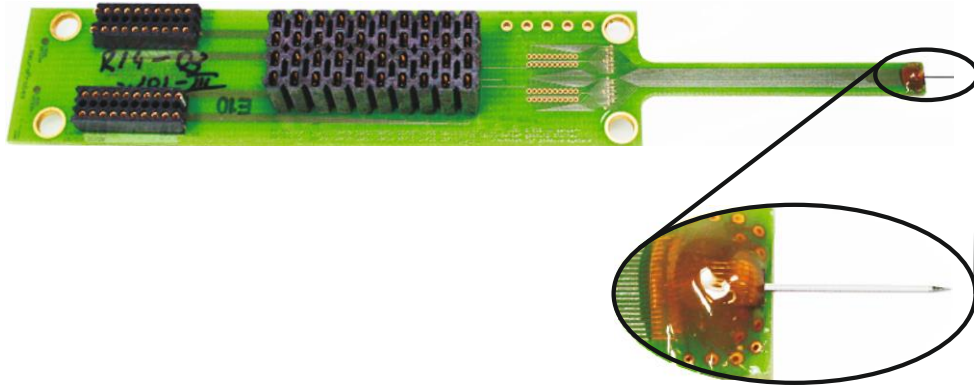


Figure 4: Assembled 4-mm-long active probe shaft and close-up of the probe bonded to a PCB encapsulated by two-component epoxy.

11 Electronic depth control software – NeuroSelect

NeuroSelect Software is used for GUI for the NeuroProbes data acquisition system, signal processing and hardware controller. Using this software, user can select up to 8 preferred electrodes, program the probe and get the signal from the selected electrodes. This software is user friendly, intuitive and easy to navigate.

NeuroSelect provides the following features:

- graphical user interface;
- communication with the hardware controller of multi-electrode probes and data acquisition;
- data processing of recorded neural signals to extract the signal quality metric;
- electrode selection based on the quality metric either in a manual or semi-automatic mode by selecting “best“ performing electrodes;
- data display, and data storage.

11.1 Graphical user interface

The NeuroSelect software provides a GUI that integrates the components for data acquisition (DAQ), signal processing and communication with the hardware controllers. The GUI is split into different windows that can be resized individually. The upper left pane is used to control the data acquisition from the DAQ card PCIe 6259 from National Instruments, as detailed later, and to define the file name for the recorded signals. The left center pane is used to configure the plot settings, i.e. data scaling and selection of electrode signals to be displayed. The neural signals acquired from the DAQ card are visualized in the main window in the center. The bottom pane gives feedback about the current status of the software as well as the hardware. The right-side window shows the control panel for electrode selection and settings. When maximizing the right pane (Figure 5), one can select the electrodes of the different probe types in a manual or semi-automatic mode.

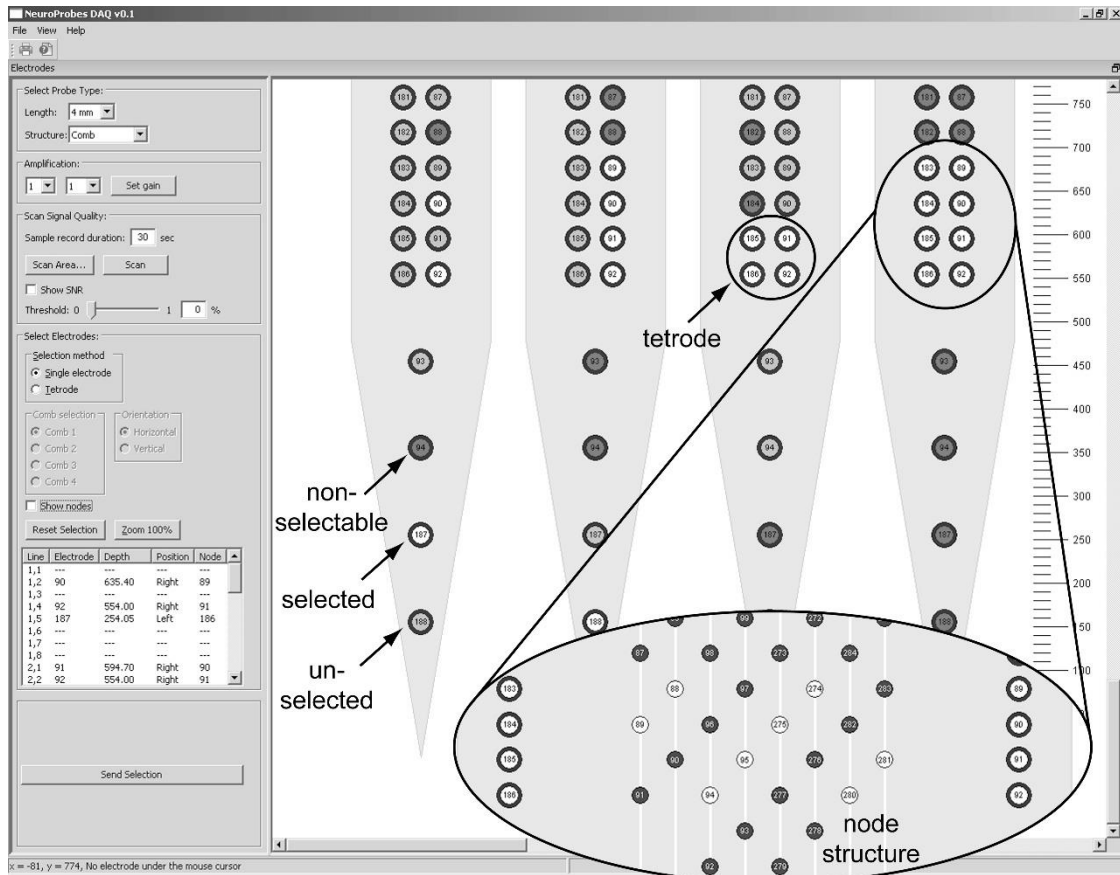


Figure 5: Manual electrode selection: Electrodes can be selected by clicking with the mouse on the electrode. Selected, unselected and non-selectable electrodes are differently color-coded.

11.2 Programming environment

The software NeuroSelect is written in C++ and uses the multiplatform framework wxWidgets distributed under free software license for the GUI implementation [66]. It is developed for Windows, but can be ported to Linux, MacOS or other platform environments. *Visual Studio* is used as main Integrated Development Environment (IDE) and compiler, but the Microsoft Foundation Classes (MFC) is not used. The design of the graphical user interface was developed using the DialogBlocks editor from Anthemion [62]. The signal analysis package is developed in C/C++ and uses the OpenMP library [65] in the parallel-processing version. This allows to use all available processors (and cores) of the computer to process multiple signals in parallel. The comments in the whole source code are written using the Doxygen format which simplifies the generation of the documentation [63]. The source code to control the acquisition hardware, i.e., the PCIe 6259 DAQ hardware from National Instruments and to visualize the neural data is generated using LabWindows/CVI from National Instruments. The development of the NeuroSelect software is controlled using the version control software Subversion.

Before development we had to consider the following business features:

1. Read the data from PCIe 6259 DAQ hardware from National Instrument.
2. Show the data to the customizable graphic.
3. Allow user to select the desired possible electrodes (up to 8 electrodes).
4. The selection method is by clicking the electrodes directly using left mouse click.
5. The selection method can be single or tetrode selection method.
6. Translate the user preferred electrodes to digital signal.
7. The needle on the user interface has the depth indicator.
8. The selected electrodes are showed on the table to simplify the navigation.
9. The software can be used to program the needle based on selected electrodes data.

Table 1 Main functions of NeuroSelect software

11.3 Programming features

The source codes are based on wxWidgets that makes possible to compile the software to Linux, Windows, Mac OS and other platforms environment. For instance, the data structure is based on wxArray and not Standard Template Library from C++ environment. This standardization is to make sure that the codes are compatible with wxWidgets.

The data acquisition is using multithreading method to avoid bottleneck from GUI system. The GUI system is slower and less important than data acquisition process. To optimize the data acquisition thread in multithreading process, it should use the dedicated processor for this process.

There is a double buffer object that is used for visualizing the acquired data to the screen. With this object, the original data from sensor remains unchanged, the visualization is faster and it ensures that the data is not changed.

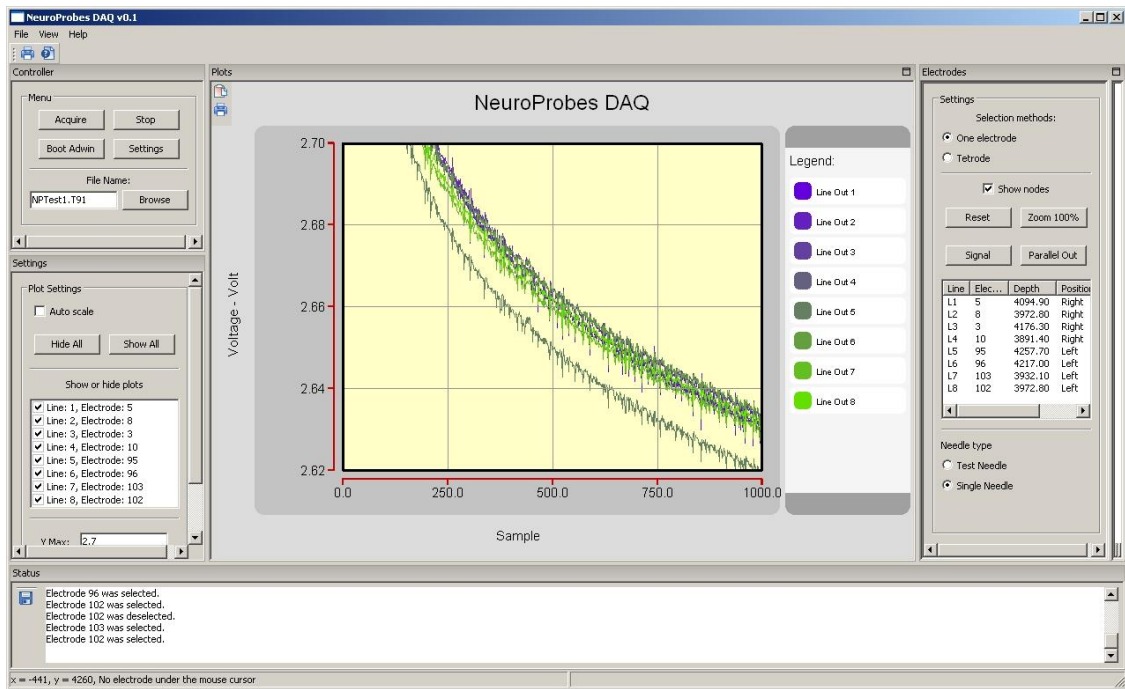


Figure 6: The main User interface from NeuroSelect Software.

The GUI that is shown above (Figure 6) is separated in several split windows that can be resized individually. The upper left pane is used to control the data acquisition from PCIe DAQ from National Instrument and set the signal file name. The left center is the plot display settings. The biggest pane on the center is the output plot from the acquired signal from PCIe DAQ hardware. We can see that the software is showing the acquired data from 8 channels. The bottom pane is the current status of the software and hardware. The right side shows the control panel for electrodes selection and settings. If the right pane is maximized, then the following two figures (Figure 7 and Figure 8) will appear depending on the setting.

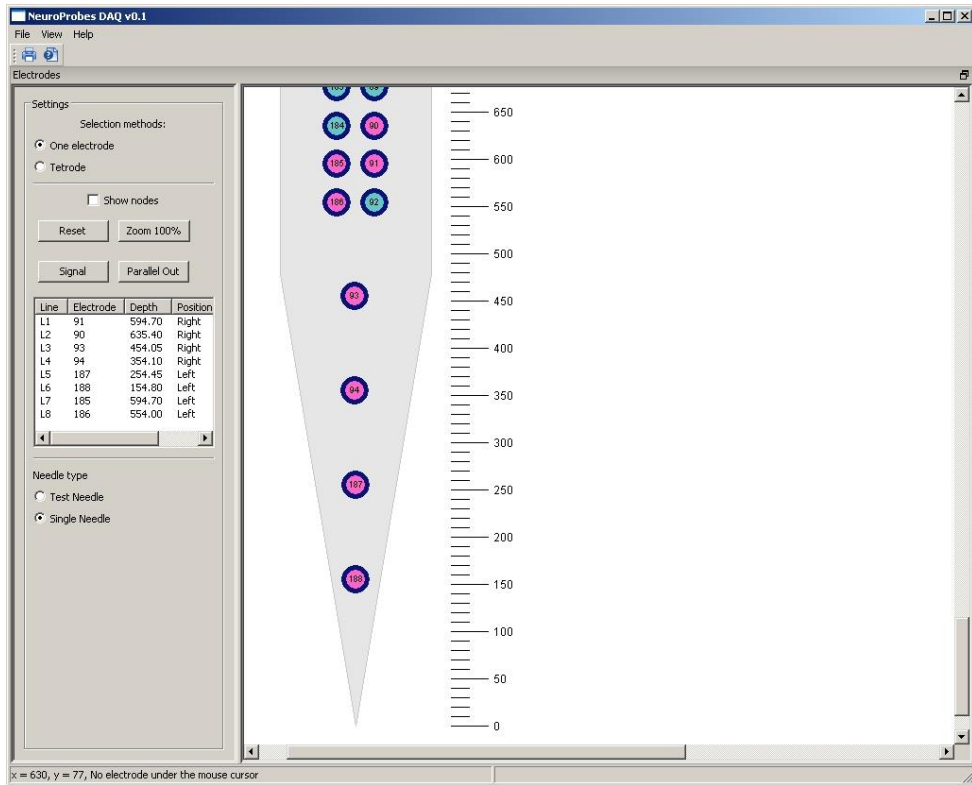


Figure 7: The selection area of the needle where user can select the preferred electrode(s).

Figure 7 and 8 display the needle with its electrodes that can be selected by the user. Due to the limitation of the number of selected electrode and the switching module configuration, therefore there are some rules in the selection. For instance, both side and left of electrodes can be selected only up to 4 electrodes and each line can be used by only one electrode. These rules are integrated within the software; user can only see that the certain electrode cannot be selected anymore.

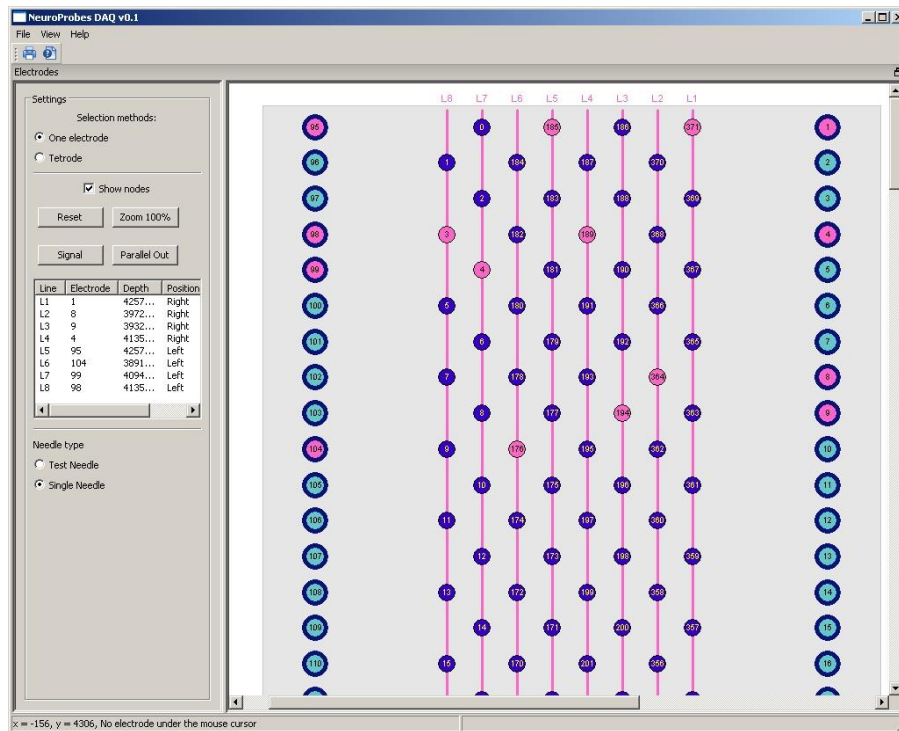


Figure 8: The selection area of the needle with the nodes is displayed.

11.4 NeuroSelect Programming Introduction

11.4.1 Data Structure of NeuroSelect Software

NeuroSelect software is based on Object Oriented Programming. The data type, structure and naming rule obey wxWidgets standard. The basis source codes of this software are generated using DialogBlocks.

Here are the data structures with brief descriptions:

Class	Description
NpApp	The application class
npControllerPanel	The control panel for electrodes
npDAQData	The data exchange container
npDAQFrm	The main frame of all windows

npElectrodeControllerPanel	Electrodes controller panel
npElectrodeNodes	Node selector
npElectrodesHandler	The handler class for electrodes
npElectrodesSet	The container for a set of electrode
npElectrodesSplitterWindow	Electrodes panel container
npElectrodesWindow	Electrodes panel
npPlot	Show the signal value using plot
npSettingWindow	Application settings
npSingleElectrode	The container for a single electrode
npStatusPanel	Show the current application status
ynPlot	The class for container of all plots
ynPoints	Class for one single plot container

Table 2 data structures with brief descriptions

Figure 9 on the next page is the collaboration diagram of this software.

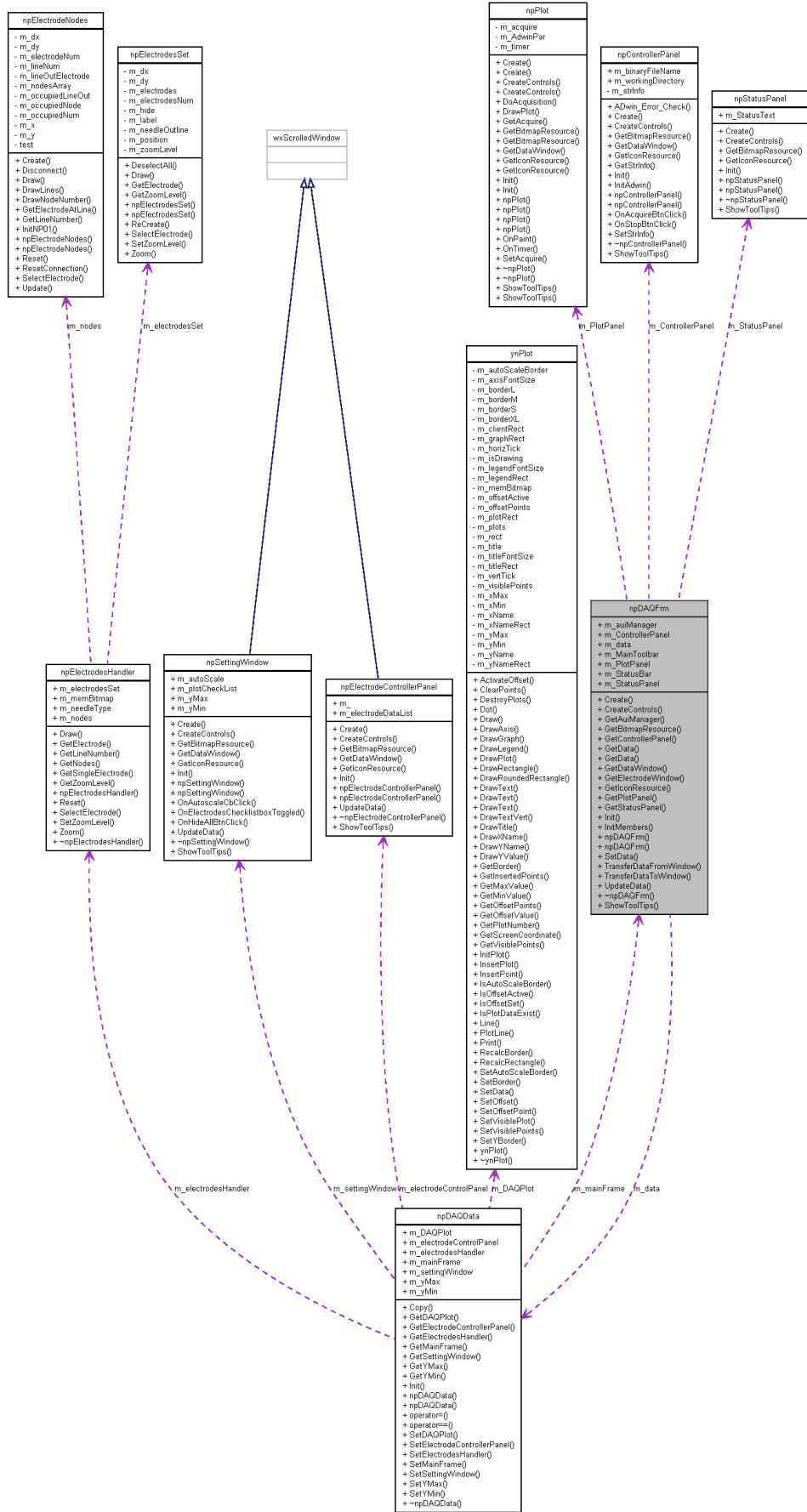


Figure 9: Collaboration diagram of NeuroSelect Software

Some objects of the NeuroSelect software are window components. The figure below (Figure 10) shows the windows with their corresponded class. They have a single object for data exchange; this object is simply a variable container object that is instantiated by the npDAQFrm object that is the main frame object. This object is based on a class which is called npDAQData. This object contains also sub window address, by knowing other windows address, each window can access the other window and performing data exchange or call other windows functions.

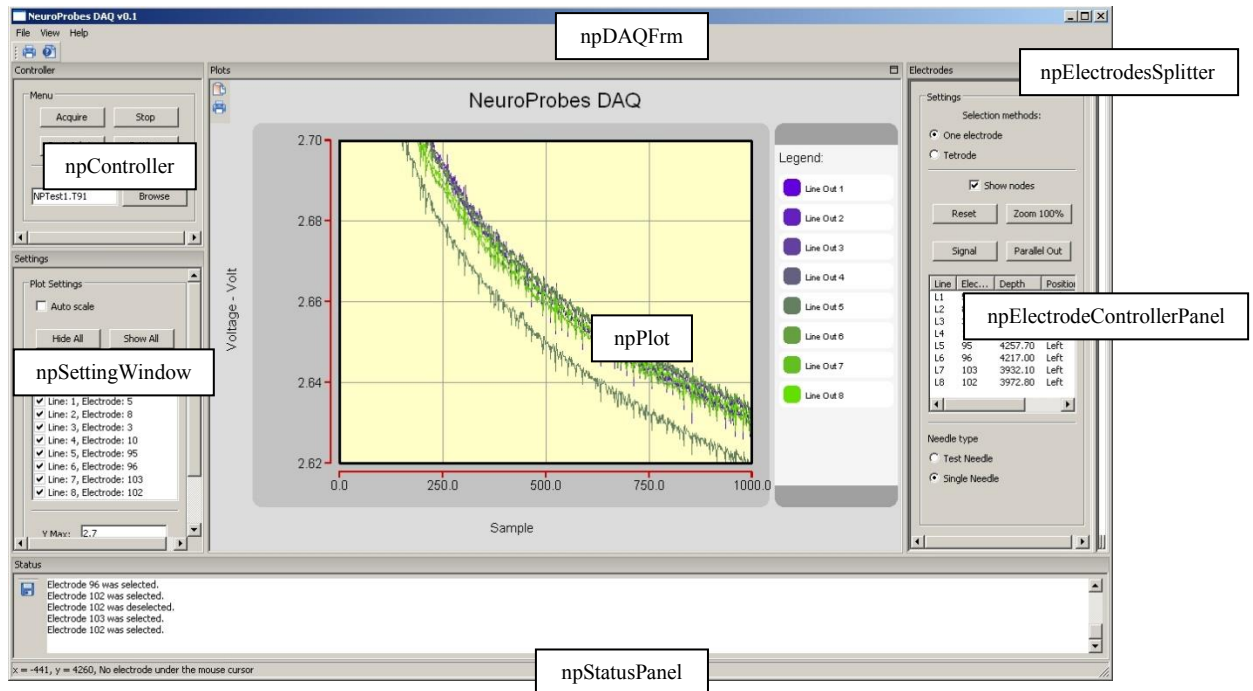


Figure 10: The screenshot of the software and its window objects

Beside GUI, the important parts of the software are the communication with hardware, data acquisition and signal processing. The source codes for data acquisition from PCIe 6259 from National Instrument are generated automatically using LabWindows/CVI from National Instrument as well. The data acquisition procedure is using multithreading process to avoid bottleneck in GUI. LabWindows/CVI can do a lot to simplify the programming process. The multithreading process is using LabWindows/CVI framework.

There are two threads in data acquisition process, the first thread is data acquisition process, save the data to the disk and copy the data to the double buffer object, the second thread is user interface (UI) thread that displays the copied data from double buffer to plot window. The UI thread is slower because it needs more calculation and calls some function display the data on the screen, otherwise working thread is only copying and saving the data.

11.4.2 wxWidgets

wxWidgets is a multiplatform GUI library for C++. C++ itself is a standard programming language for many operating systems like Windows, Linux, Mac OS and some more. Based on wxWidgets allows NeuroSelect source code is compiled to several platforms as mentioned above. There is another variant of multiplatform GUI like QT. We used wxWidgets because it is free, more Rapid Application Development (RAD) software available and similar with MFC. Some MFC classes are corresponding with wxWidgets, for instance wxString and CString, wxDocument and CDocument, wxBitmap and CBitmap and some other more.

wxWidgets is only a C++ library and not a compiler, therefore we need a compiler and IDE to use with wxWidgets. In this project, Microsoft Visual C++ from Visual Studio was the main IDE and compiler to develop this software. This compiler has many facilities to debug, watch the value of variables, step debugging and Intellisense which simplifies and makes faster the software development. Using Visual C++, the wxWidgets source code can be compiled in smaller size compared with other windows compiler.

The first version of NeuroSelect software has been compiled successfully on Mac OS platform. The software is depending on the hardware PCIe DAQ hardware library that currently focused in the Windows version, therefore the current software cannot be compiled to other operating system, like Mac OS. For the future, we should adapt this software to other possible operating system that is supported by PCIe DAQ hardware.

Developing a complex user interface using wxWidgets is not difficult because there are several available RAD softwares and some of them are free. DialogBlocks from Anthemion considered to be the best from all of them, because it supports most of the wxWidgets UI components, especially the most important component, like wxUI and wxSize that beautify NeuroProbes UI.

11.4.3 Anthemion DialogBlocks

DialogBlocks is a RAD or visual programming software, based on wxWidgets. We can create wxWidgets components like buttons, windows, splitters, menus and other supported components by wxWidgets (Figure 11).

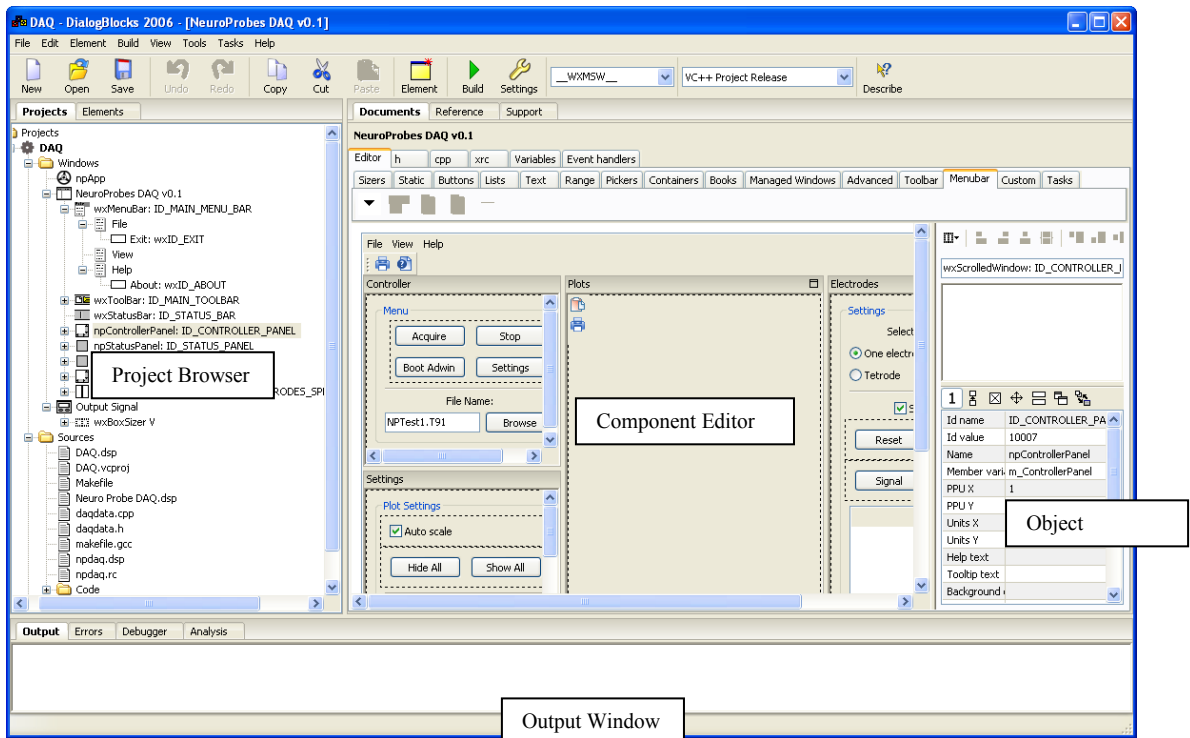


Figure 11: Screenshot of Anthemion DialogBlocks

11.4.4 Subversion

The development of the NeuroSelect software was controlled using version control software, Subversion. This software controlled the change of the source code. If the new code generates bugs, we can revert to the current source code to the last stable code. We can also see who changed the source code and the reason why they changed it. Subversion can be used for single user or multiuser and computer all over the world as long as they have access to internet.

Subversion can be divided to two parts; those are server and client side. The server side stores the committed data to the disk, save the changes that were made by the users. These changes are saved to keep the track of the software development.

11.4.5 Doxygen

Doxygen is a documentation software for Java and C++. This software parses the comments in C++/Java code to the structured documents on several formats like HTML, Latex, and some more. The generated documents contain functions, classes, variables, defines, constant and others standard C++/Java keywords. Relation between classes and files are also possible displayed using a relational graph.

The codes development that will be documented using Doxygen must follow Doxygen rules in giving the comments in the codes.

11.5 Data acquisition

As each CMOS-based neural probe shaft provides eight analog output channels, 32 and 128 signals are provided by the 4-comb and 4×4 platform arrays, respectively. These signals are pre-amplified using a custom-made CMOS amplifier and fed to the data acquisition cards, i.e. PCIe 6259 DAQ from National Instruments with 16-Bit resolution, sampling rate of 31.25 kHz per channel and up to 32 analog inputs. Four of these cards are required to acquire all signals from a full 4×4 platform; one is sufficient for a single comb. The auxiliary digital inputs (available on a connector to the interface electronics) can be treated like an additional analog channel. Data are acquired in blocks of 4096 samples, which correspond to the European Data Format (EDF) block size as the described later.

11.6 Electrode selection

Prior to any data acquisition, the user has the choice between different probe types. So far, probes with different shaft lengths, i.e. 2-mm-, 4-mm- and 8-mm-long probe shafts, and different probe configurations, i.e. single-shaft probes, probe combs with four probe shafts or 3D probe arrays comprising 4×4 probe shafts, are under development within the NeuroProbes project and can be selected within the NeuroSelect software. Furthermore, the amplification for the CMOS-based pre-amplifier is set in this window of the GUI. The probe type selection is followed by the electrode selection mode as schematically shown in Figure 12. The user can choose between a manual electrode selection mode and a semi-automatic mode. While the semi-automatic mode is supported by data analysis and corresponding calculation of the quality metric, all possible electrodes might be selected in the manual mode.

11.6.1 Manual electrode selection mode

Up to 8 electrodes per shaft can be selected by mouse clicking on the electrode symbols of a single-shaft probe, a single comb or the combs of a 3D 4×4 array as shown in Figure 5. In case of the whole array, the user can select within two-dimensional planes, i.e. each plane comprises all shafts of one 4-shaft comb or each plane comprises corresponding probe shafts of four different combs. The selected and non-selected electrodes are color-coded as indicated in Figure 5. Further, the user has the possibility to either choose single electrodes or tetrodes, i.e.

a set of 2×2 neighboring electrodes. As already described, each electrode can be switched to one out of two output lines as illustrated in Figure 12 (A). Thus, only a certain selection of single electrodes is possible. The rules based on this interconnection scheme are implemented in the software and non-selectable electrodes are disabled for user selection and are again color-coded. The corresponding node structure of the electrode selection matrix can be visualized if required (cf. inset in Figure 8).

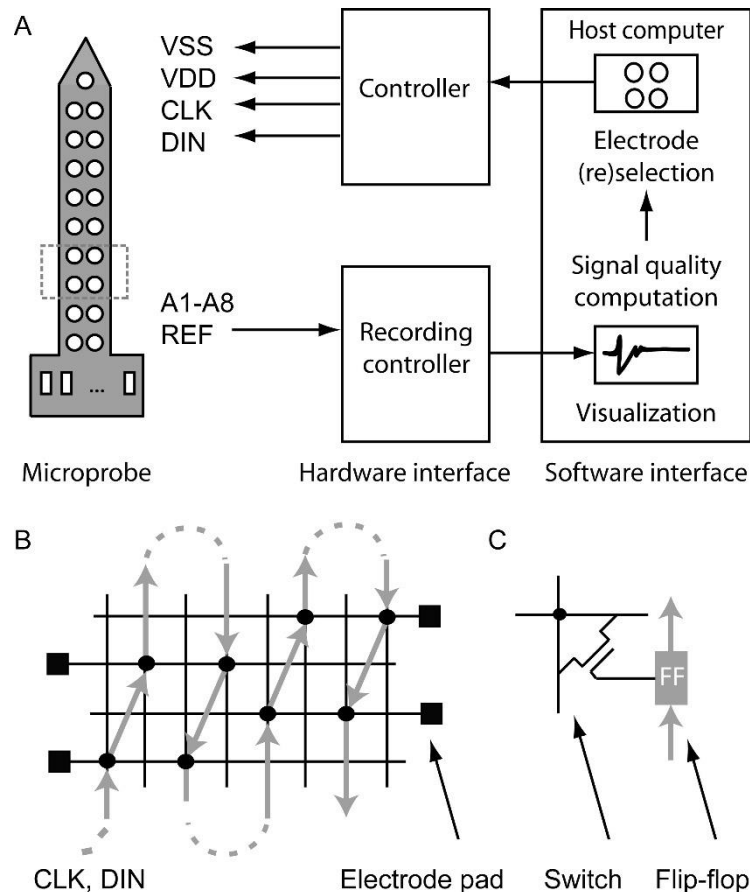


Figure 12: Closed-looped system design: (A) Electrode selection is transferred from the host computer via a controller to the microprobe. Neural signals are recorded and visualized. Based on the computed signal quality the electrodes are (re)selected. Selection is achieved via a shift register comprising flip-flops (FF): (B) Elementary cell of switch matrix, (C) single node with switch and FF.

11.6.2 Semi-automatic electrode selection mode

In the previous section, I presented the manual electrode selection mode of NeuroSelect software. In some cases, the manual selection takes very long time to scan the whole probe in order to find good quality signal. Thus, my goal was to fully automatize the electrode selection and in the first step I integrated a semi-automatic solution which contains an algorithm, developed by the Catholic University of Leuven. The automatic electrode selection mode, as a second step remains a future development plan, therefore in this dissertation I present only the

semi-automatic version of the software. As shown in the program flow chart in Figure 13, the semi-automatic scan comprises a selection of blocks of 8 electrodes per shaft of which signals are recorded during a user defined time and saved in the EDF-format. The signal quality metric, i.e., the SNR, is calculated for each block of electrodes as described later. The recording time is adjustable and requires a stabilization time of 30 seconds for the applied CMOS-based pre-amplifiers. To reduce the total recording time, the user can constrain the scanning area by selecting a coarse section of the probe in which the electrodes are scanned. The results of the SNR computations are visualized by color-coded electrodes, so the experimenter can see immediately the electrodes with probably good unit activity. It is possible to adjust the lower limit of the distinguished SNR values in the GUI. Based on the information of the signal quality, the user finally selects the appropriate electrodes manually.

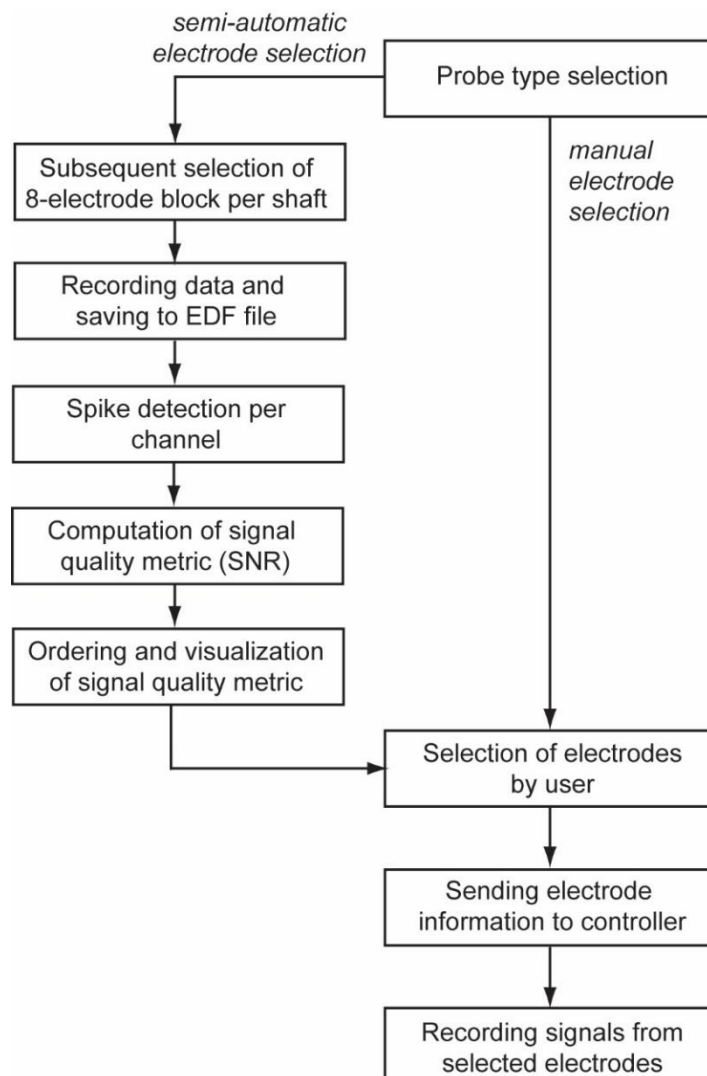


Figure 13: Data visualization and program flow-chart of manual or semi-automatic electrode selection.

For visualization, the LabWindows/CVI library from National Instruments was used. A visualization of the recorded data as a superimposed view of single spikes with the computed SNR and firing rate in real time is currently under development.

11.7 Data saving

The recorded signals are saved under the user defined file name in the EDF specified in Ref [64]. The EDF consists of a code to create the standard headers defining the number of channels etc., and the code to write the sample data to the file. The latter works very efficiently together with the data acquisition card, because the National Instruments DAQ library was used to collect exactly one block of 4096 samples for all 33 channels (32 analog channels + 1 digital channel) per data acquisition card directly into memory. Because this memory buffer already has the right data structure, it can then be written in a single disk write call to the EDF file. The header file is written with “-1” (unknown) in the number of data records during acquisition. This header field can be filled in with the correct number only after the acquisition has been finished.

11.8 SNR metric for spike quality assessment per channel

The NeuroSelect software includes a powerful SNR calculation for the EDC probes. Here I want to note, that my contribution to the SNR functionality of NeuroSelect software is restricted to the integration part, nonetheless I would like to show it in a few sentences.

Using the detected spike windows and the signal as input, the SNR is computed as the relative power of the spikes compared to the background noise. Once the spikes are detected, the root mean square (RMS) of all samples within the window (cf. rectangles in Figure 14) around a spike stamp (cf. circles in Figure 14) is computed. The RMS values of all detected spike windows are then averaged. The width of the windows should be taken over the whole time interval of a spike. As an example, the width of the time windows in Figure 14 was set to $t_{tw} = 1$ ms. The SNR value is calculated as

$$SNR_{dB} = 20 * \log_{10} \left(\frac{\overline{RMS}}{\sigma_{noise}} \right)$$

where \overline{RMS} and σ_{noise} denote the average root mean square of the spikes and the standard deviation of the noise, respectively, calculated by the RMS of all mean centred values outside the spike windows which are the pure noise segments.

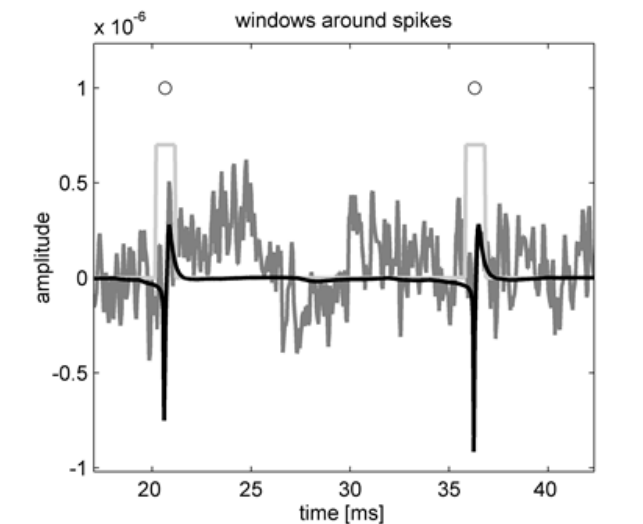


Figure 14: Spike detection - Rectangle windows of a width of 1 ms are centred around detected spikes (spikes with negative deflections in this example). Black signal is the underlying ground truth signal, after adding the real noise from the probe the signal in gray is obtained. Spikes need to be detected from this noisy signal, the underlying ground truth signals provides information on the correctness of the detection.

11.9 Perspectives of future developments

In one hand, the earlier mentioned fully automatic selection mode of the control software is not just a convenience functionality, but it also includes serious potentials towards the brain-computer interfaces. In this case, the algorithm always selects the electrodes with the best SNR, ensuring stable connection with the outer world. It follows that it would be necessary to modularize the software, in order to use its main functionalities, like recording, saving, visualization, SNR calculation and electrode selection, etc. as an independent component.

On the other hand, although my version of the software does not support the next functionality, the probe itself is theoretically capable to connect more than one transmission gate into one line, thus creating a bigger recording surface. Increasing the recording surface would be useful to improve the quality of multiunit activity.

12 Neural signal processing

This section presents commonly performed signal processing methods. It focuses on recent developments appropriate for multi-electrode arrays with an increased spatial resolution allowing to extract higher level information of the brain neural networks.

Below I investigated the necessary spike sorting algorithms and time-frequency analysis methods in order to select the best fitting ones for the in-vivo validation of EDC probes.

12.1 Spike sorting and clustering

Spike sorting is a signal processing technique to assign single unit activities recorded by a multielectrode to a corresponding neuron. Further, it is a prerequisite for studying many types of brain function and a big technical challenge too. In this chapter I will present what the spike sorting is, what kind of problems are rising when someone try to use it and finally I will review the main clustering algorithms. The main steps of spike sorting are summarized in Figure 15.

The neurons are communicating with each other with APs. We can record them with an electrode, but in this case, we measure from multiple neurons' activity, in other words, we record multiple unit activity, so somehow we should differentiate them. Depending on the goals of the experiment, the neurophysiologist may wish to sort these signals by assigning particular spikes to putative neurons, and do this with some degree of reliability. In most of the cases the essential of the measurement is that we connect the measured firing to a neuron with proper reliability. Often it is hard to differentiate between spikes from single neuronal activity, especially when we calculate with the impacts of noise, external effects or similar firing patterns of the surrounding neurons. Even the simple solutions, like thresholding, can often change the result, for example, it can shift to the direction of a neuron with higher amplitude. The spike sorting algorithm can help in the separation of neurons which are close to each other, even if they are firing synchronously.

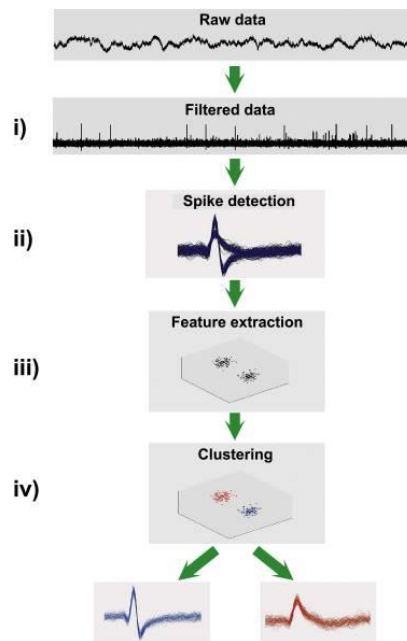


Figure 15: Basic steps of spike sorting. Step i) The continuous raw data is band-pass filtered, e.g. between 300 Hz and 3000 Hz. Step ii) Spikes are detected, usually using an amplitude threshold. Step iii) Relevant features of the spike shapes are extracted, thus giving a dimensionality reduction. Step iv) These features are the input of a clustering algorithm that performs the classification. Adapted from [117]

Measuring electrode picks up the surrounding voltage which biggest component is the field potential and in up-state the APs are visible. Other interfering factors are the local cumulation of signals and AP like noises from neuronal fibers which are seem like APs, but most of them are eliminated by filtering, although it is important to mention that, in some cases, axons and axon terminals can also give separable signals. Later I will not discuss it in detail, but here I would like to mention that I didn't find any axon or axon terminal like spikes in the signal, recorded from the somatosensory cortex. Nevertheless, beside the one shaft 4mm probe, which is the subject of this dissertation, a four-shaft version of the electronic depth control probe also exists and with the latter probe, the ongoing experiments found axonal spikes in the capsula interna and ventrobasal complex (nRt spikes). Back to the properties which affect the spike detection, the size of the tip of the electrode (in case of single wire electrode type) or the measuring surface of the electrode can influence the measurement, because if the measuring surface is bigger, then the detectable number of neurons will be more, but the separation and sorting of the cell firings are going to be more difficult. If the measuring surface of electrode is too small, then the thermic noise of electrode is higher, so the separation of APs is much more difficult to pull out from noise. The nature of the neural activity in one measurement can be change, even with the decreasing amplitude of the APs. The movement of the neural tissue is a similar artifact. It is a frequent case when under the implantation of the electrode, the brain tissue can be pressed in and later on comes back to the original position [119].

One interesting question is that if we have multiple APs with different shapes, are they coming from one cell or their origins are completely different? How can we distinguish signals coming from the cumulation of noise from neurons which are in local field but they are farther and how can we compare the latter with real APs? How can we separate overlapping APs?

In the following subsections I will give a short introduction to spike sorting algorithms from the simplest to the more complex.

12.1.1 Threshold detection

In an ideal case, on the measured signals, the APs show a good characterized shape. Unfortunately, this is not true most of the cases, because the shape of the firing of a neuron can be change under one measurement. The set of the voltage threshold is the most often used threshold detection method. It is very important to set a value for threshold which is certainly enough to clearly separate the noise from the AP. One main feature of most of the shape of firings is the amplitude, so with thresholding with the proper value, the APs who are step over this value, are highlighted. The main advantage of this technique is the minimal software and hardware requirement, but sometimes it can result with poor quality of isolation. We can use correlation diagrams between firings for checking purposes which can show the connection between firings, so if the firing is in the refractor period then the separation is not right. It is often impossible to set the threshold which is capable to take difference between the background activity (firing of neurons in the local environment) and the noise. So it is worth to give threshold to optimizing the found false positive and false negative firings.

It can lead to other problems, if the opposite component of noise in the same time wipes out the background firing, then it does not reach the threshold and we cannot detect it. This is a big problem when a neuron fires rarely, so we can lose lot of information. Another opportunity is when two neurons in the background fire in the same time so their amplitudes are detectable cumulatively and we are getting a different activity shape which can step over the threshold.

12.1.2 Differentiating spikes

There are lots of possibilities to make difference between APs, such as, based on the height or width of spikes, or the peak-to-peak amplitude. The use of these solutions, we can cluster spike patterns based on appropriate properties.

Another option is to use principal component analysis (PCA). Many attempt to recognize patterns resulted with bad outcomes, because of inappropriately selected relevant

elements. The PCA is automatically searching for the needed shapes, in such a way that they should create orthogonal base. Every spike is sorted to its maximum point, so the shape of the spikes shows minimum variability, in that way we can reach the best differentiation. The PCA algorithm assigns a ratio to every spike, which comes from the score of firing and its principal components. The score of the principal components depends on how much variability they represent. We can get the principal component vectors from the calculation of the unit vectors of covariance matrix. The two highest scored components are enough to define the shape of spikes, because other components have much lower values compared to the beforementioned two highest ranked components.

12.1.3 Clustering algorithms

The simplest solution for clustering is based on amplitude, but it is not capable to handle the firings with decreasing amplitude in long term.

12.1.3.1 K-means based clustering

The abovementioned cell sorting algorithms can show how should be split spikes into clusters by hand, but automated processes also exist for that. Simpler versions are the K-means algorithms, which evolve clusters by their mean, more precisely the algorithm classifies the points into clusters by the Euclidean distance calculated from mean values. In every iteration, it compares the other points to the actual mean values and at the end of iteration it modifies the place of mean values based on their associated actual points. The algorithm stops when the places of mean values are not changing on consecutive iterations. The algorithm only uses the information from the mean values and does not consider the distribution of data within the cluster. This approach is sufficient and appropriate if clusters are well separated, but it doesn't work if clusters are significantly overlapped or the shape of the cluster is substantially different from spherical distribution.

12.1.3.2 Bayesian clustering

The Bayesian clustering method observes the groups by their statistical distribution [119]. The Bayesian clustering has multiple data model. In case of neural AP classification, the multivariate Gaussian distribution is a popular data model for Bayesian clustering, therefore in the next, I assume that the clusters are multivariate Gaussian distributed. The likelihood of the data given a particular class c_k is given by:

$$p(x | c_k, \mu_k, \Sigma_k)$$

where x is the spike data vector, μ_k is the mean value and Σ_k is the covariance matrix for class c_k . Based on the Bayesian rule, classification is performed by the calculation of probability of the data point belongs to each of the classes.

$$p(c_k|x, \theta_{1:K}) = \frac{p(x|c_k, \theta_k)p(c_k)}{\sum_k p(x|c_k, \theta_k)p(c_k)}$$

This defines the models Bayesian decision boundaries implicitly, because the cluster membership is probabilistic and the boundaries of cluster are given as a function of confidence level. The parameters of the classes are optimized if we maximize the likelihood of the data

$$p(x_{1:N}|\theta_{1:K}) = \prod_{n=1}^N p(x_n|c_k, \theta_{1:K})$$

12.1.3.3 Expectation maximization clustering

Expectation maximization (EM) algorithm suppose a Gaussian distribution of the clusters, based on the claim that for a given cluster the spike variability is determined by additive and Gaussian stationary background noise [50]. In case of EM algorithm given a probability function $L(\theta, x, Z)$, where θ is the vector of parameters, x is the observed data and Z is representing the missing data (not observed data). The marginal probability of observed data $L(\theta, x)$ defines the estimation of maximum likelihood. The EM algorithm is searching for the estimation of maximum likelihood of marginal probability with the iteration of next two steps [50].

Expectation step: calculating the expected value of likelihood function based on conditional probability of Z , to a given x observation for $\theta^{(t)}$ actual estimated parameters.

$$Q(\theta|\theta^{(t)}) = E_{Z|x, \theta^{(t)}}[\log L(\theta; x, Z)]$$

Maximalization step: find the parameter which can maximalize the next expression:

$$\theta^{(t+1)} = \arg\max_{\theta} Q(\theta|\theta^{(t)})$$

The SUA data - recorded by EDC probes - was analyzed by competitive EM-based clustering algorithm [50] using custom-made Matlab software.

12.1.4 Open problems in spike sorting practice

Spike sorting is a very challenging mathematical problem that has attracted the attention of scientists from different fields. It is indeed an interesting problem for researchers working on signal processing, especially those dealing with pattern recognition and machine learning techniques. It is also crucial for neurophysiologists, since an optimal spike sorting can dramatically increase the number of identified neurons and may allow the study of very sparsely firing neurons, which are hard to find with basic sorting approaches.

Given the extraordinary capabilities of current recording systems - allowing the simultaneous recording from dozens or even hundreds of channels - there is an urgent need to develop and optimize methods to deal with the resulting massive amounts of data. The reliable identification of the activity of hundreds of simultaneously recorded neurons will play a major role in future developments in neuroscience.

In the previous section of this dissertation I have introduced the main issues of spike sorting. However, there are still many open problems, like the sorting of overlapping spikes, the identification of bursting cells and of nearly silent neurons, the development of robust and completely unsupervised methods, how to deal with non-stationary conditions, for example, due to drifting of the electrodes, how to quantify the accuracy of spike sorting outcomes, how to automatically distinguish single-units from multi-units, etc. One of the biggest problems for developing optimal spike sorting algorithms is that we usually do not have access to the "ground truth". In other words, we do not have the exact information of how many neurons we are recordings from and which spike correspond to which neuron.

12.2 Fourier and wavelet transformations

For the examination of temporal, spectral, and spatial properties of the SO I used Fast Fourier and wavelet transformations. In the next sections I give a short introduction to these transformations to a better understanding why I used them to validate EDC probes.

12.2.1 Displaying biological signals

The Fourier transformation (FT) can be used for non-stationary signals. If we want to know what the spectral components of the signal are, but we do not want to know when they were happened. Nevertheless, if we would like to know the time of a specific spectral component, so when did that happen, then, FT is not the best choice. To solve this problem, we have to apply a transformation, which can represent the time- frequency map of the signal.

Among others, Wavelet transformation is suitable for this task, so it gives the time- frequency resolution of the signal (There are other methods, like Short Time Fourier transformation, Wigner distribution, etc.).

12.2.2 Fast Fourier Transformation

In order to better understand the concept behind the Fast Fourier transformation (FFT) we should know what the Discrete Fourier Transformation (DFT) is. Why do we care about the FT? Physically it will tell us the frequency components of our function or signal. Most functions are composed of many different frequencies. And mathematically it is often simpler to manipulate the function in the frequency domain. We speak of decomposing a function into its frequency components in the Fourier domain. The FT of a continuous time signal $x(t)$ is defined as:

$$X(\omega) = \int_{-\infty}^{\infty} x(t)e^{-j\omega t} dt, \quad \omega \in (-\infty, \infty).$$

The DFT replaces the infinite integral with a finite sum:

$$X(\omega_k) \triangleq \sum_{n=0}^{N-1} x(t_n)e^{-j\omega_k t_n}, \quad k = 0, 1, 2, \dots, N-1$$

In the field of digital signal processing, signals are processed in sampled form, so we don't need to speak more about the continuous FT. DFT is simpler mathematically and more relevant computationally than FT. FFT refers to an efficient implementation of DFT. When computing the DFT as a set of N inner products of length N each, the computational complexity is $O(N^2)$. When N is an integer power of 2, an FFT algorithm delivers complexity $O(N \lg N)$, where $\lg N$ denotes the log-base-2 of N , and $O(x)$ means 'on the order of x '. So FT requires lot of multiplication: N^2 multiplication is needed for the transformation of N number. For DFT of a series, this contains 1000 measured points need one million multiplications. If the data is divided into two equal parts, then the transformation of the two parts separately costs $2(N/2)^2$ multiplications. If the partial result of two transformations easily be combined, then FFT is the right choice. It is also clear, that N could be practically the integral power of 2.

12.2.3 Wavelet transformation

It has been shown that a satisfactory measure of phase synchrony as phase-locking can be obtained with wavelet transformation [81]. A wavelet in short is a wave form which is restricted in time and its average is zero. The sinusoidal waves are not restricted in time, they spread from minus infinite to plus infinite. Out of that, sinusoidal waves are smooth and regular, wavelets are assymmetric and irregular. As we discussed earlier, Fourier analysis is about decomposing the signal into frequency components. Similar to this, wavelet analysis means to decompose a signal into versions of scaled and shifted components, originated from a mother wavelet $\psi(t)$. It is important to select this mother wavelet according to the task. Mathematically the scaling and shifting of the mother wavelet means:

$$\Psi_{b,a}(t) = \frac{1}{\sqrt{a}} \Psi\left(\frac{t-b}{a}\right) \quad a, b \in R > 0$$

where $\psi(t)$ is the mother wavelet, b is the shift, a is the scale parameter. It is clear that if the a parameters' value starts to decrease, then the wavelet is more localized into the spectral range and increasingly suitable for analyzing high frequency signals.

A wavelet splits the frequency-time plane into a $\Delta f * \Delta t$ sized cell. In this spectral range the usual time- and frequency range representation is a special resolution, when the given cell is infinite in one way (more precisely it covers the whole observed spectral range or rather the whole observation time). Of course we can experiment on the phase plane with infinite resolution. The question is that why wavelets are better than other basis functions? While frequencies of wavelets are relatively well-defined, meanwhile their temporal position are restricted too. These two conditions – because of similar reasons to the quantum mechanical uncertainty relation – are not satisfied simultaneously with arbitrary precision.

We explain the signals by their orthogonal basis function. If they are Dirac-delta functions, then we get to the usual amplitude-time description. If they are sine or cosine functions, then it is the Fourier description.

The base structure of wavelet transformations consists of recursive filterings and (as it was mentioned in the FFT section) sorting of even – odd members.

Wavelets need relatively low (comparable with FFT) computation capacity. The discrete wavelet transformation (DWT) compared with FFT is relatively a fast sequence, which transforms a 2^N sized input vector (sequence) into an output vector with the same size. So that both of FFT and DWT are actually a rotation from the amplitude - time range to the frequency-time space and both of them can be described by a matrix.

12.2.4 Spectrogram for state locked changes in EEG

To visualize mean up- or down-state locked changes in spectral power over time in a broad frequency range, we used a custom-made matlab software. Calculating a baseline-normalized spectrogram requires computing the power spectrum over a sliding latency window then averaging across data trials [33]. The calculated power in dB at given frequency and latency relative to the time locking event can be visualized with a predefined color for every image pixel [33]. For the spectral estimate computation of one epoch at a given frequency and in a given time, we used either short-time Fourier transform or a sinusoidal wavelet.

13 Biological results

13.1 General remarks

In the scope of the current study, we investigated the LFP, multiunit activity (MUA), SUA, and spectral signatures of the SO. More specifically, we identified the spatiotemporal and spectral properties of SO-related LFP and SUA/MUA, and the phase relationship of the LFP and SUA/MUA during SO, and compared these observations to the existing knowledge to justify the use of the EDC device.

13.2 Implantation procedures

Wistar rats ($n = 5$, weight of 250 - 350 g) were used for the experiments. All procedures were approved by the Animal Care Committee of the Institute of Cognitive Neuroscience and Psychology, Research Centre for Natural Sciences, Hungarian Academy of Sciences, Budapest, Hungary. Initial anesthesia was administered through intramuscular injection of a mixture of 37.5 mg/ml ketamine and 5 mg/ml xylazine at 0.2 ml/100 g body weight; temperature was maintained at 37 °C throughout the 1 - 4-h-long recording sessions. The anesthesia was maintained with successive updates of the same drug combination of 0.2 ml/h. Animals were placed in a stereotaxic frame (David Kopf Instruments, Tujunga, CA, USA), and craniotomy was performed over the trunk region of the primary somatosensory cortex (S1) anterior-posterior: (AP: -1.0 -4.0), medial-lateral: (ML: 1.0 + 4.0), with respect to the bregma [112]. The probe was attached to a manual microdrive (David Kopf Instruments) through its mounting PCB (Figure 16), and it was slowly (0.1 mm/s) inserted in the S1 trunk region AP: -2.6 mm, ML: 2.5 mm with respect to the bregma driven by hand. The probes usually penetrated the dura and pia mater without bending, breaking, and causing significant brain dimpling or visible bleeding. After recording from the trunk region of S1 for 1– 4 h, the probe was withdrawn and the animal was sacrificed.

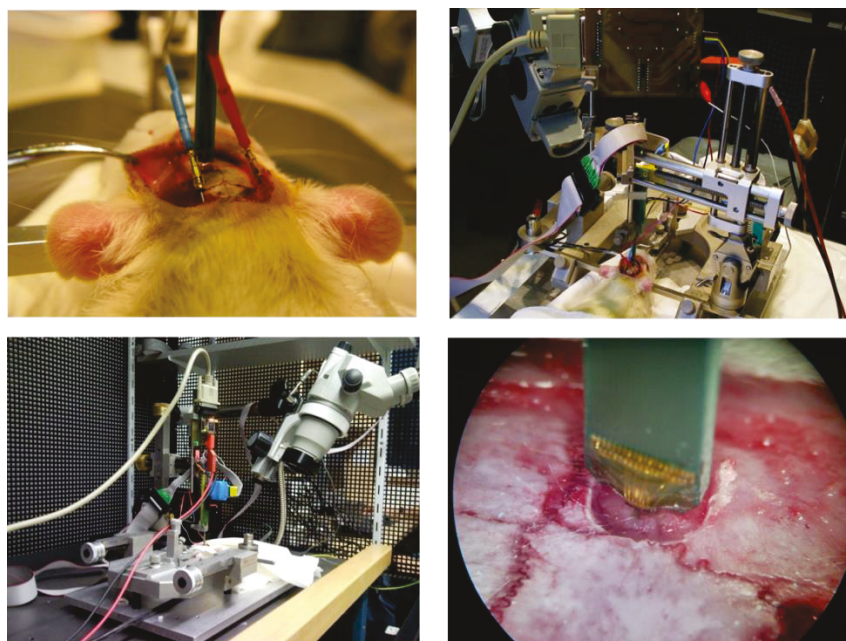


Figure 16: Implantation procedure; Animals were placed in a stereotaxic frame. Stainless-steel needle ground and reference electrodes were placed on the left and right side of the craniotomy. The probe was attached to a manual Microdrive through its mounting PCB. The EDC probe was implanted under the surveillance of a surgical microscope, so we were able to verify the depth of the implantation.

13.3 Neural data recording procedures

Before the implantation, impedance measurements were carried out to confirm the integrity of the probe, using 250 nA, 1 kHz sine wave as testing signal (EASI-1; BAK Electronics, Mount Airy, MD, USA) injected into selected recording sites. The measurements were done in Ringer's lactate solution (TEVA, Budapest, Hungary) against an Ag/AgCl reference electrode. In all cases, the impedances were measured between 0.5 and 1 MOhm for the functioning electrode sites. The impedance measurements were also repeated while the probe was implanted in the brain, with roughly similar results (data not shown). The outputs of the EDC probe were fed into a highinput impedance referential preamplifier (bandwidth of DC-100 kHz, gain = 10). Stainless-steel needle ground and reference electrodes were placed on the left and right side of the craniotomy. Wide bandwidth electrical activity (0.1 - 7000 Hz) with an overall gain of 1000 was recorded (with custom-made filter amplifier) at 20 kHz/channel sampling rate, on eight channels, with 16-bit precision (PCI6259, LabView; National Instruments, Austin, TX, USA) and stored in hard drive. To extract the LFP, the wideband data were further band-pass filtered at 0.1 - 500 Hz, 24 dB/oct, zero phase shift. To extract SUA and MUA, the raw data were further band-pass filtered at 500– 5000 Hz, 24 dB/oct, zero phase shift offline using NeuroScan Edit 4.3 software (Compumedics, El Paso, TX, USA). The recording site selection was sent to the EDC probe through the FPGA-based controller using the NeuroSelect GUI software.

13.4 Temporal, spectral, and spatial properties of the SO

LFP recordings were conducted with the EDC probe from the trunk region of the primary somatosensory area ($n = 8$ penetrations). A representative example of the LFP and MUA depth profile is shown in Figure 17A spanning the whole cortical thickness approximately evenly in Figure 17B and D, respectively. The time series of SO was characterized by the rhythmic recurrence of positive and negative half-waves in the recorded LFP traces (Figure 17B). Close to the surface, up-states (darker gray shading) were characterized by large positive deflections crowned by higher-frequency (spindle and gamma range) LFP oscillations (channels 1 – 3 in Figure 17B), while in the cortical depth, the up-states were negative, and the trough of the wave was also characterized by higher-frequency oscillations. The down-states (lighter gray shade) were negative in LFP recording close to the cortical surface and inverted into positivity in the deeper layers. Multiple unit firing (Figure 17D) and higher-frequency oscillations were low in all layers of the cortex during down-states. The frequency spectrum of the oscillation was calculated using the FFT algorithm. The LFP data were cut into 8192-ms-long segments and averaged in the frequency domain using cosine window smoothing. We found that the average peak frequency of the SO was usually in the 1 – 2 Hz range (Figure 17C). As the EDC probe was implanted under the surveillance of a surgical microscope, we were able to verify the depth of the implantation by counting the recording contacts outside of the brain. To evaluate the spatial pattern of the LFP phase inversion, we recorded from eight roughly equidistant locations from the depth of the cortex spreading all layers, separated by approximately 300 μm . We found a clear LFP phase inversion of the SO in all of our recordings. The phase inversion was usually located between 300 and 600 μm depth measured from the pia mater (Figure 17B, contacts 2 – 4).

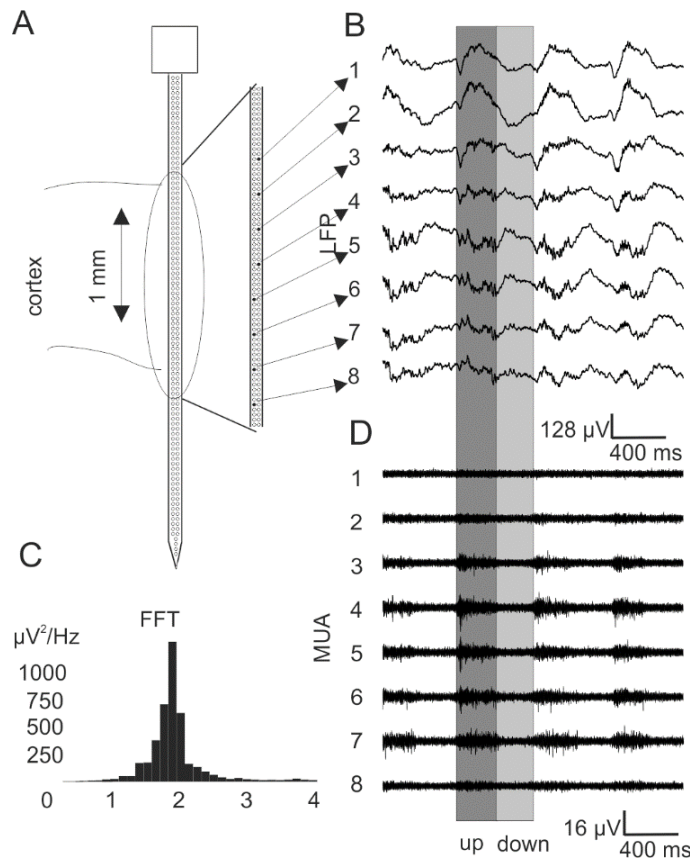


Figure 17: (A) Approximate recording position of the 4-mm long, active probe in the cortex. Close-up of eight roughly equidistant recording locations separated by approximately $300 \mu m$. (B) Example LFP traces from the eight recording locations. Rhythmically recurring positive (dark gray) and negative (light gray) half-waves are highlighted. (C) FFT of the LFP spectrum. (D) Example MUA traces from the eight recording locations. The original raw data were bandpass filtered between 500 and 5000 Hz.

13.5 Detection of up- and down-states

To evaluate the electrophysiological features of the SWA, it is indispensable to analytically define up- and downstates. To obtain an estimate on the timing of the state transitions, we defined the up- and down-state onsets by using MUA measures. According to previous studies, extracting the envelope of the MUA helps identifying state transitions. To extract the MUA envelope, first the wide band signals were band-pass filtered (500 – 5000 Hz, 24 dB/octave, zero phase shift) and rectified (Figure 18A). On the resulting traces, an additional low-pass smoothing filter was applied (30 Hz, 24 dB/octave, zero phase shift) to obtain the envelope of the signals (Figure 18B). In the next step, the up- to down-state and down- to up-state transitions were defined (Figure 18C). First, we identified the largest up-state/down-state amplitude ratio channel, which was usually located in layer V. Down-states were manually defined, a marker was placed in the deepest trough of the down-state, and the average and standard deviation (SD) of these points were calculated. We defined the state transition thresholds as the average plus two SDs. If two upstates or two down-states were separated by

<100 ms, the two states were extended and merged together. To test if this threshold measure had a meaningful physiological explanation, the amplitude histogram of the MUA envelope was constructed. In all of the cases, this histogram was found to be bimodal, indicating the presence of two processes, more specifically the up- and down-states of the oscillation (Figure 18D). In addition, the calculated threshold value was always located between the two peaks of the bimodal distribution.

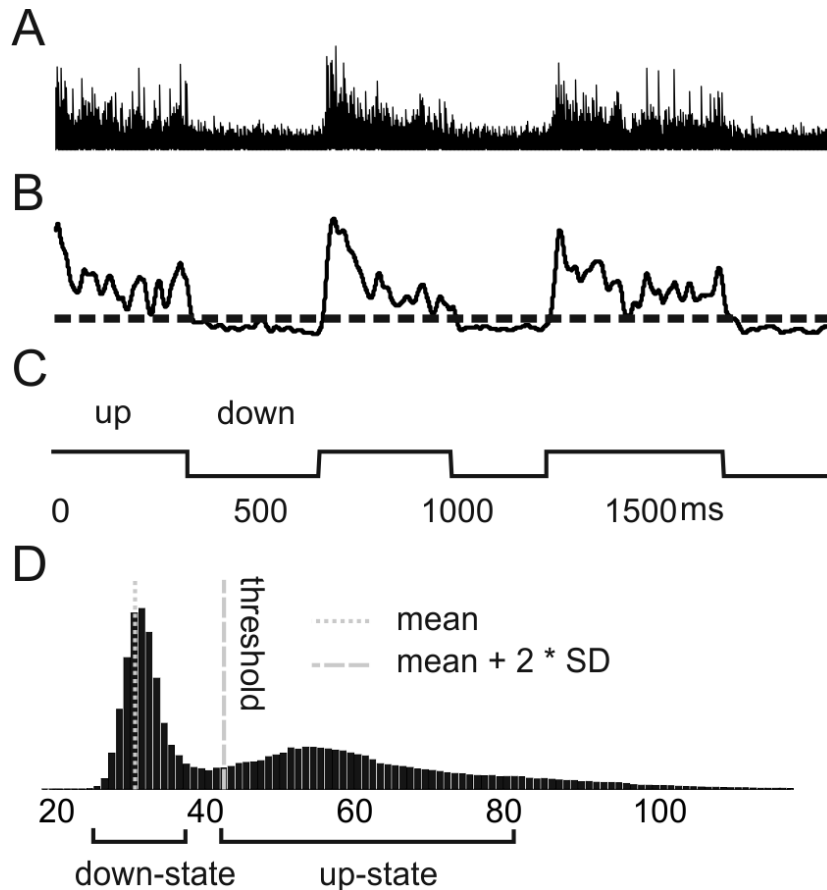


Figure 18: State detection based on MUA. (A) Example MUA trace obtained from raw data by band-pass filtering (500 – 5000 Hz) and rectifying (arbitrary units). (B) Low-pass-filtered (30 Hz) MUA used for state detection. (C) Result of state detection based on the low-pass-filtered MUA in B. (D) Amplitude histogram of MUA envelope.

13.6 Averaged depth profiles of the SO

By using the time stamps of the down- to up-state transition as a reference point, the average spatial, temporal, and spectral patterns of the SO were calculated to relate our measurements to the findings of other results using different probes [23, 30, 124]. We found that the up-state locked, averaged LFP profile showed an amplitude inversion at the third contact located around 600 μm below the pia (Figure 19A). The corresponding MUA depth profile showed maximal amplitude on the fourth or fifth electrode corresponding to 900–1200 μm

cortical depth (Figure 19B). Joint time-frequency analysis was performed on the recorded LFP data using wavelet-based methods [33]. The spectral content of the oscillation was calculated from single sweep LFP waveforms followed by averaging of the resultant individual time-frequency measures. Dividing the wavelet amplitude values with that of a distant baseline (-1000 to -500 ms) in each frequency band gives the relative change of spectral activity in time expressed in dB. We found that up-states were characterized by increased oscillatory activity mainly in the gamma range (30 – 80 Hz) in all of the layers, while in the down-state the spectral activity was decreased in all layers (Figure 20).

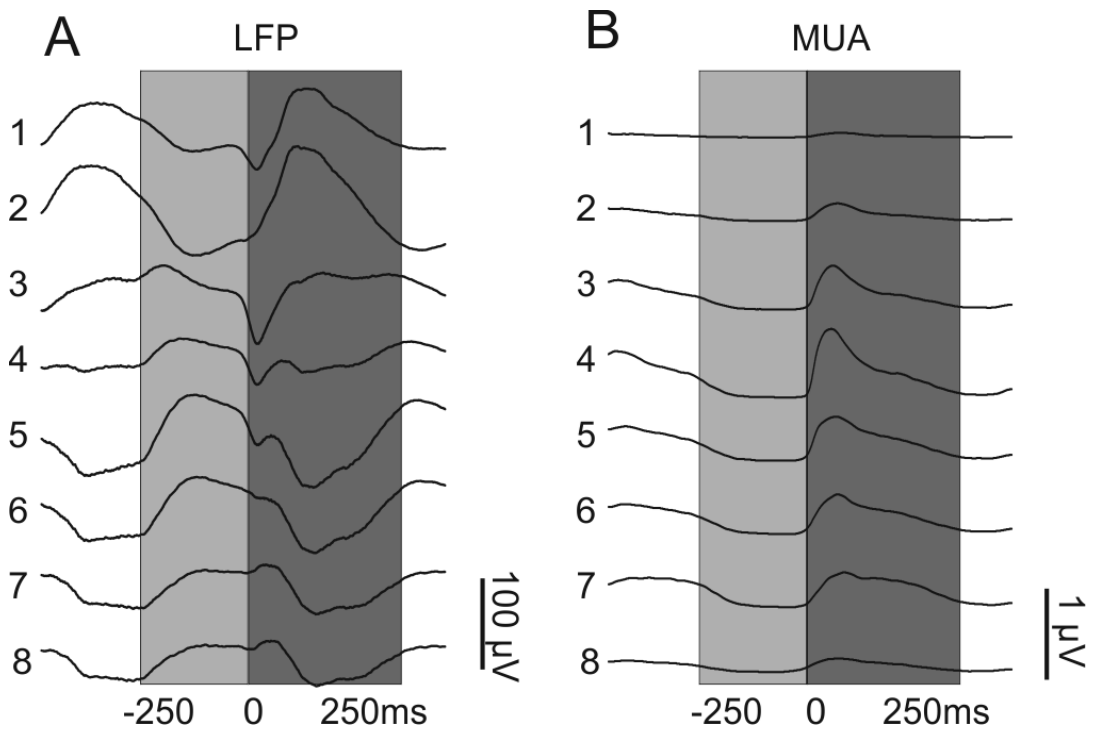


Figure 19: Up-state locked averages. (A) Up-state locked averaged LFP traces recorded from the eight locations (see close-up in Figure 17A). Amplitude inversion between contacts 2 and 3 corresponding to an approximate recording depth of 600 μ m. (B) Up-state locked averaged MUA traces. Maximal amplitude on contacts 4 – 5 corresponding to an approximate recording depth of 900 – 1200 μ m. Light shading indicates downstate; dark shading indicates up-state.

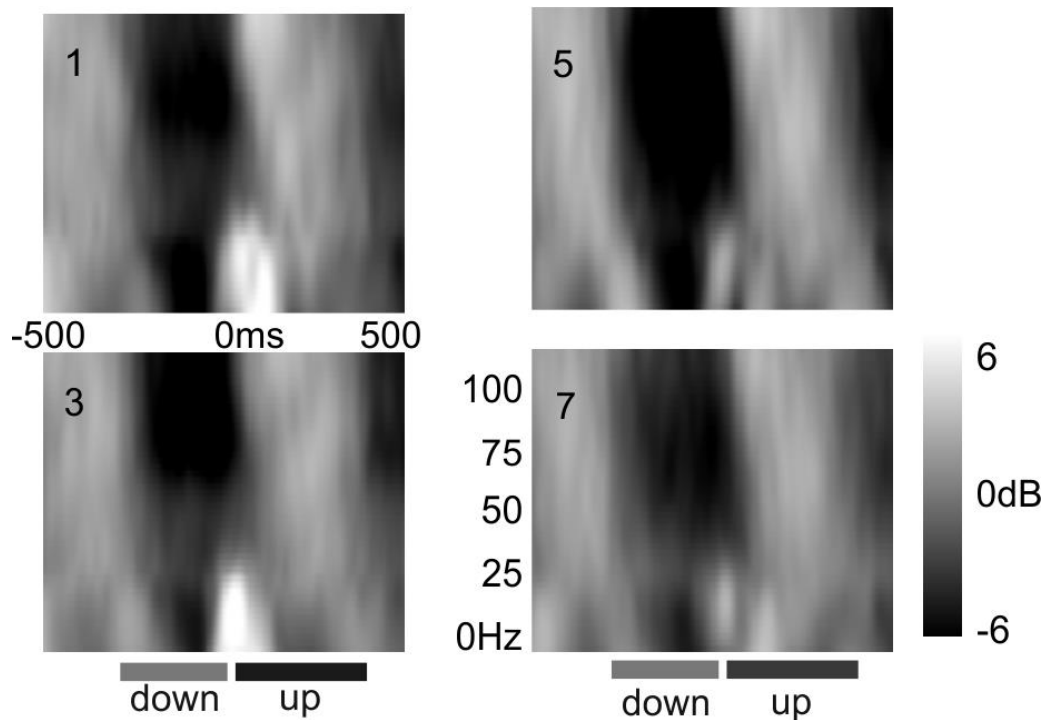


Figure 20: Average time-frequency maps of up-state locked epochs on selected recording channels 1, 3, 5, and 7 separated by approximately 600 μm . See close-up in Figure 17A for distribution of recording channels (1 – 7) along the probe shaft. Increased (light colors) oscillatory activity in the gamma range (30 – 80 Hz) during up-state and decreased (dark colors) spectral activity during down-state in all layers.

13.7 Properties of SUA

Putative SUA was analyzed by filtering, threshold detection, and clustering methods using custom-made Matlab software. The wide-band signal was further digitally filtered (500–5000 Hz, zero phase shift, 24 dB/octave, in Neuroscan Edit 4.3) to eliminate low-frequency contamination of the AP data (Figure 20A). After threshold recognition [32] at a given channel (mean \pm 3 – 5 SD, each channel separately), two representative amplitude values (e.g. peak and trough) were assigned to each unclustered AP waveform. These duplets were projected into the two-dimensional space (Figure 21B), and a competitive expectation-maximization-based algorithm [50] was used for cluster cutting [52] (Figures 21C and D). If the autocorrelogram (Figures 21E, F, and G) of the resulting clusters contained APs within the 2-ms refractory interval, it was reclustered. If reclustered did not yield a clean refractory period, the AP was regarded as originated from multiple cells and omitted from the single cell analysis. We found that the clustered single units exhibit an autocorrelation profile that reveals mostly three main oscillatory processes. Unit bursting at fast time scales (200 Hz) is visible in Figure 21E, spindle activity (8– 17 Hz) is revealed in Figure 21F marked with a single asterisk, while the SO is pointed out at a longer recurrence rate corresponding to about 1.5 Hz frequency (Figure 21F,

double asterisk). Interaction between two separated single units is visible on the cross-correlogram (Figure 21H) revealing about the same 1.5 Hz recurrence rate as in Figure 21F.

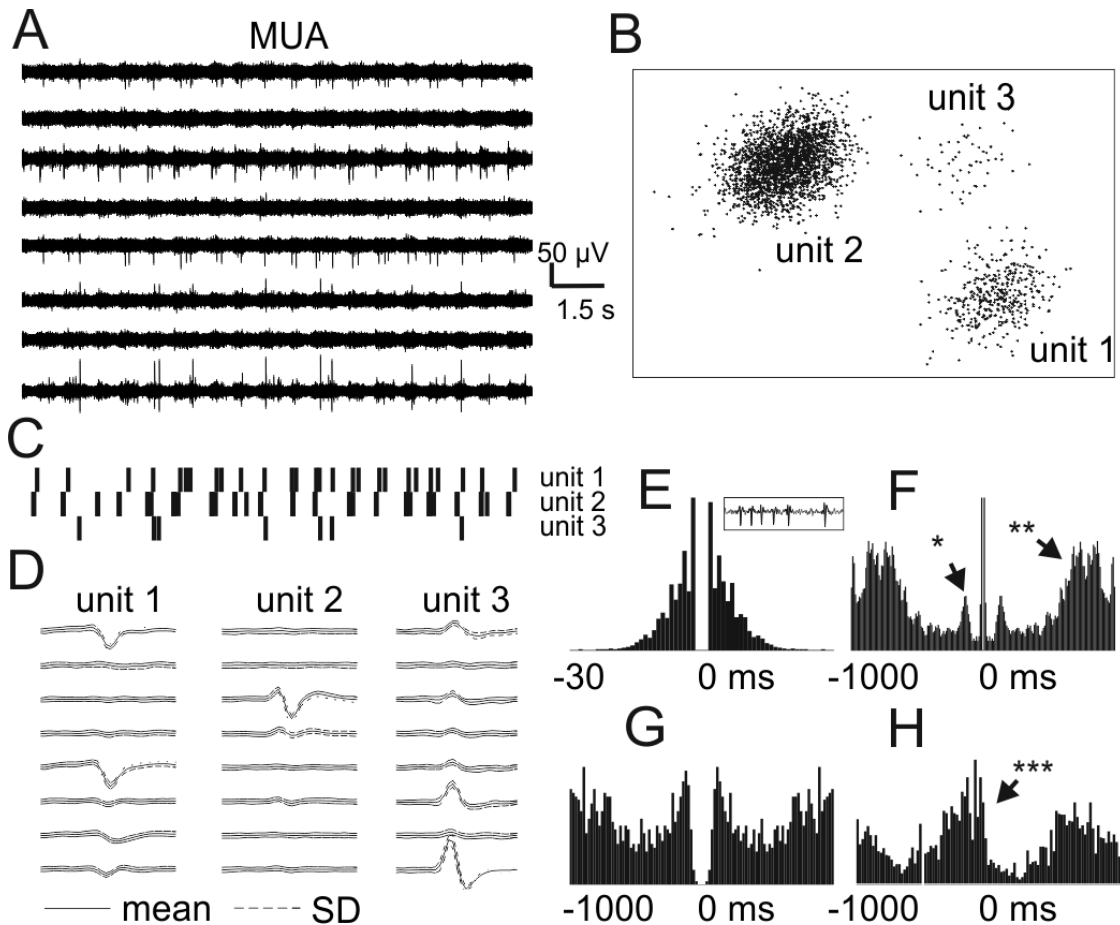


Figure 21: (A) Representative SUA traces. (B) Isolated clusters of three units from A. (C) Raster plots of the three isolated units in B. (D) Mean spike waveforms with SD of the three isolated units in B along the eight recording channels (Figure 17A). (E) Autocorrelogram of unit 2 firing. Inset: burst firing of unit 2. (F) Autocorrelogram of unit 2 firing with longer time scale. (*) marks spindle modulation and (**) marks SO modulation of unit firing. (G) Autocorrelogram of unit 1 firing. (H) Cross-correlogram of unit 1 and unit 2 firing. (***) marks SO modulation in the cross-correlogram.

To further characterize the relationship of sorted unit firing and LFP phase, both up- and down-states were individually (sweep by sweep) divided into 10 phase bins and the corresponding sorted single unit firing was depicted on a histogram. The results of such analysis are depicted in Figure 22, where three separated single units are related to the phase of the SO. We found that most of the firing is happening during the up-state of the SO, and only a minor activity is taking place in the silent phase. To test the temporal stability of the recording system, if a putative single unit was found at a given site, the probe was configured using the NeuroSelect software to record from a distant location. After usually 5 – 10 min, without moving the device, the probe was reconfigured to the location where the single unit was originally found. In all of the attempts ($n = 5$), we were able to find the same putative single unit, proving the

reliability of the recording site switching software, hardware, and the stability of the probe within the cortex.

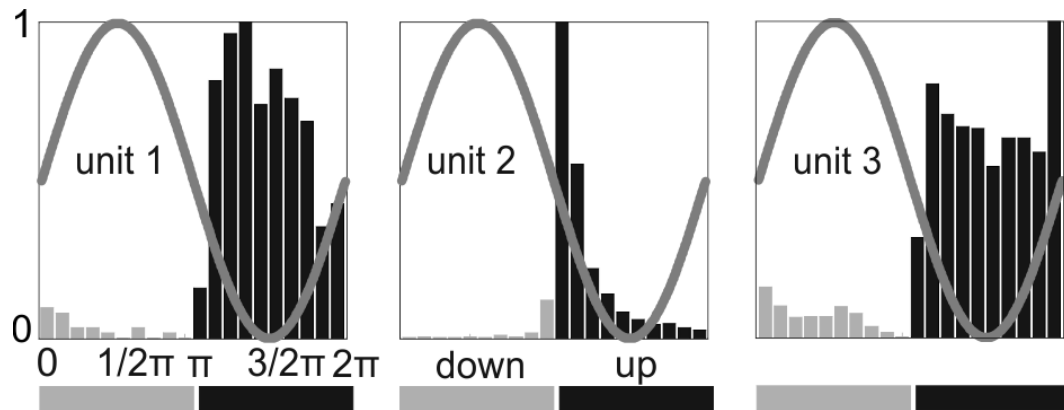


Figure 22: Phase histograms of three representative unit firings related to the phase of SO. Phase bins are represented on the horizontal axis and normalized firing rates are represented on the vertical axis. Light bars indicate down-state; dark bars indicate up-state. In all three cases, unit firing mostly occurs during up-state, while during down-state only minor unit activity is observed

13.7.1 Firing patterns of single unit activities

Under the recording sessions I found multiple firing patterns, e.g. high frequency firings at the beginning of the up-state, or uniformly firing activity during the event (Figure 22.), but I didn't examine them in details. Nevertheless, other experiments have been showed that these behavior types can be generalized and based on this, neurons can be classified into different classes [85]. It has been observed, that under ketamine-xylazine anaesthesia, recording from the somatosensory cortex of the rat's brain, spontaneous activity periods can be classified into the next classes:

- Long-term up-states, which are in context of traveling waves. Interneurons are showed higher firing rates in the first 100 ms of the event, then they were returned to a constant level to the end of the up-state. Pyramidal cells were not so active at the onset of up-state, but this level of activity was preserved long-term [85].
- Another type was the so called simultaneous onset up-state, which take less time, modulated with sharp field potential and ripple frequency (~ 12 Hz) oscillations. These were rhythmically occurred in delta frequencies (~ 3 Hz) and may be thalamocortical interactions play a critical role in the generation of these oscillations. Interneurons showed strong activity in the simultaneous onset up-states, synchronized to the ripple frequency, while Pyramidal cells were not showed in average ripple frequency modulation [85].

Although, each Pyramidal cell and interneuron showed difference in their relative latch on to up-state, however, activation order of the cells were similar [85].

14 Conclusions

In this dissertation, I summarized the general features of sleep, mainly slow oscillations, the recent implantable brain electrical recording systems and introduced the mathematical basis of time- frequency analysis and spike sorting techniques. Based on these, I have described a novel electrophysiological recording system comprising one shank silicone probes with a high number of recording sites. The recording system applies a novel concept, the electronic control of recording sites, to gather data in an effective way. The effectiveness of this system was proven in multiple experiments conducted in rats. The EDC probe performs well for recording both the unit activity and the local field potentials.

The EDC system demonstrated here is suitable for acute experiments, it provides stable multi- and single-unit recordings for hours. One of the advantages of the electronic depth control approach compared to passive probe arrays is that recording sites containing high quality unit activity can be dynamically selected (selecting areas with the best signal-to-noise ratio) which in turn improves the single unit yield of the experiments. That is, we do not have to record from recording sites which provide no useful data, therefore we can keep the amount of recorded data reasonable as well. The densely placed recording sites are optimal for unit recordings and separation of the recorded unit activity into single unit clusters. The spatial information of the recorded action potentials can be used to perform a reliable spike sorting procedure.

Another advantage of the electronic depth control is that after the initial implantation the probe does not have to be moved physically until the end of the acute experiment. In case of tetrode recordings or recordings with passive silicon probes, the amplitude of the spikes of the recorded single units can significantly decrease over time (e.g. due to electrode drift) or even disappear (e.g. due to the death of the neuron), preventing the separation of the action potentials of these particular single units. In this scenario, passive multielectrodes have to be moved to new positions to try to follow the single units or find new neurons located close to the electrode. However, the mechanical translation increases the chance of severe tissue damage and bleeding. Using EDC probes we only have to select other recording electrodes to find single units or areas of interest, thus reducing the probability of severely damaging the tissue around the probe.

I also presented the NeuroSelect software for managing the electronic depth control of cerebral CMOS-based microprobes for extracellular in vivo recordings. NeuroSelect makes it possible to scan the electrodes electronically and to select, or reselect those electrodes of best signal quality resulting in a closed-loop design of a neural acquisition system. Electrodes can be

selected in a manual or semi-automatic mode based on the signal quality. In addition to managing communication with the hardware controller of the probe array, the software also controls acquisition, processing, display and storage of the neural signals for further analysis.

In conclusion, the EDC devices are capable of fulfilling the experimental demand aimed toward a versatile probe system that is capable of rapidly reconfigurable, mass neuronal recording while avoiding mechanical damage to the brain due to physical motion.

Finally, I would like to highlight my personal contribution to the EDC project. NeuroProbes and NeuroSeeker projects consist of several consortium partners, and each partner employed lot more scientists. In addition, each project can be further divided into several subprojects. The EDC project was one of them. My work basically consisted of 3 major parts. First, the development of the EDC microelectrodes had the highest priority and I did not contribute to it, but it is indubitable that these electrodes, because of they are active, cannot work without a control software. As part of a team, I was responsible for the design, integration of algorithms, test and validation of this control tool. Second, when the hardware and software part was ready to test, our lab had the chance to try them first in the world. I actively contributed to this challenging task, namely with the design of the experiments, the electrode and recording system setup, surgical procedure and data collection. Third, when we finished with the experiments and collected the appropriate amount of data, I had to show to the consortium, that the electrode setup is usable in practice. For the validation, I chose an unconventional way, namely to prove the usability of the EDC probes via the SO of the brain. I did this, because our lab was basically worked on SO related projects and it follows that I had the proper domain knowledge to complete the validation. In addition, we developed multiple Matlab based algorithms from spike sorting to time-frequency analysis that were also presented in this dissertation and I also added my work to that projects.

15 Novel scientific results

Thesis group I.

Software control of electronic depth control silicon probes

I.1. I have enabled to the experimenters to control and effectively use the CMOS-based neural probes in neurophysiological experiments through an intuitive tool.

This tool enables the experimenter to visualize the recorded signals, the spikes, as well as the calculated metrics like the SNR value per electrode and their relative ordering with respect to each other. This tool also manages the recording of the signals through the DAQ PCIe 6259 card from National Instruments, the storage of these signals into EDF files, the execution of the SNR calculation algorithms, and the steering of the electronic circuitry to record from the electrodes when selected manually or semi-automatically.

Publication related to thesis group I: [I]

Thesis group II.

In vivo electrophysiology with the electronic depth control silicon probe

II.1. With the aid of the EDC probe, I was able to detect both states of the SO with high reliability using LFP, MUA/SUA, and spectral measures.

More specifically, I found that the LFP is rhythmic at about 1 Hz; its depth profile well corresponds to our previous findings, where the LFP inversion was taking place in layer III corresponding to a depth about 300– 500 μm below the cortical surface.

II.2. With the aid of the EDC probe I have shown that the bimodality of the oscillation using MUA measures can be reliably characterized, which is also in correspondence with the basic properties of SO and previous findings.

In addition, similar analysis techniques can be implemented on the EDC data as they were used on data obtained by the classic silicon probes. Besides LFP and MUA measures, another characterizing feature of SO is the spectral signature of cortical electrical activity indexed by an LFP spectrogram. Previous investigations showed large cortical oscillatory power in a wide frequency band (10 - 200 Hz) during up-states, while the spectral power was much smaller during down-states. My findings are in a perfect match with these reports.

- II.3. Consistent with prior studies in animals, I have shown with the aid of the EDC probe that the up-state was associated with increased firing and elevated spindle and gamma power during the surface-positive LFP half-wave, while the down-state was characterized by the widespread surface-negative LFP half-wave with decreased firing, and oscillatory activity.**

Single unit clustering ability is another key feature of silicon probes, in general.

- II.4. I found that the EDC probe is capable of recording well-sortable single units, and these clustered cells show similar properties as similarly processed records of classic silicon probes.**

- II.5. I have shown that reliable unit detection and search is possible with the EDC system by just switching between the recording channels rather than moving the device in the brain.**

Publications related to thesis group II: [II, III]

In conclusion, I have shown that the EDC system is an equally capable device to record brain activity as existing silicon probe implementations. In addition to the classic devices, it has the ability to map large areas of cortical fields without being physically moved, which makes this device a unique tool for less invasive neural recordings. Owing to the fast and non-invasive reconfiguration of recording contacts, the EDC device may significantly increase the amount of information that can be obtained during a single experiment as compared with passive silicon probes.

16 Acknowledgements

Conducting my Ph.D. thesis research within the European FP6 NeuroProbes and FP 7 NeuroSeeker project was a real pleasure that brought me the invaluable experience of working at the fascinating interface of electrophysiology and neuroscience. To investigate and implement control software for neural systems and apply them in in-vivo experiments with possible benefit for humans, although in the far future, was truly inspiring.

In particular, I would like to thank Prof. Dr. György Karmos and Prof. Dr. István Ulbert for giving me the opportunity to pursue my Ph.D. thesis at Faculty of Information Technology and Bionics of the Péter Pázmány Catholic University. I am very grateful for their guidance of my scientific development. I sincerely appreciate their valuable comments and inspirations that challenged me to go further in my research.

I further would like to thank my advisor Prof. Dr. István Ulbert for his helpful comments and suggestions during the whole time. I am very thankful for providing me his knowledge and giving many suggestions. Furthermore, I express my gratefulness for his tremendous effort in performing the in-vivo experiments using the EDC probes. His openness for new technology and his talent in both, neuroscience and engineering, have been the key of the successful experiments.

I am very thankful to Dr. Karsten Seidl and Dr. Patrick Ruther for their contribution to the NeuroProbes project, including probe designing, fabrication, NeuroSelect software designing. Special thanks to Dr. Karsten Seidl for his exceptional effort in performing the in-vivo experiments.

I also thank to my colleagues Dr. László Grand, Dr. Richárd Cserecsa, Richárd Fiáth, Dr. Bálint Péter Kerekes and Dr. Lucia Wittner for their help during these in-vivo recordings.

For their contributions to the software development, I particularly would like to thank Yohanes Nurcahyo, Dr. Karsten Seidl and Dr. Richárd Cserecsa.

The work was supported by the Information Society Technologies (IST) Integrated Projects NeuroProbes of the 6th Framework Program of the European Commission, NeuroSeeker of the 7th Framework Program of the European Commission and the Hungarian National Brain Research Program.

Sincere thanks are given to Péter Kottra for his assistance in the surgeries.

And finally I would like to thank all of my colleagues of the laboratory not mentioned yet for their support in many aspects and for providing a very pleasant and inspiring atmosphere.

17 Publications

17.1 Author's publications related to the dissertation

- [I]. Dombovári B, Fiáth R, Kerekes BP, Tóth E, Wittner L, Horváth D, Seidl K, Herwik S, Torfs T, Paul O, Ruther P, Neves H, Ulbert I. In vivo validation of the electronic depth control probes. *Biomed Tech (Berl)*. 2014 Aug; 59 (4):283-9. doi: 10.1515/bmt-2012-0102.
- [II]. Seidl K, Torfs T, De Mazière PA, Van Dijck G, Csercsa R, Dombovari B, Nurcahyo Y, Ramirez H, Van Hulle MM, Orban GA, Paul O, Ulbert I, Neves H, Ruther P. Control and data acquisition software for high-density CMOS-based microprobe arrays implementing electronic depth control. *Biomed Tech (Berl)*. 2010 Jun; 55 (3):183-91. doi: 10.1515/BMT.2010.014.
- [III]. Torfs T, Aarts AA, Erismis MA, Aslam J, Yazicioglu RF, Seidl K, Herwik S, Ulbert I, Dombovari B, Fiath R, Kerekes BP, Puers R, Paul O, Ruther P, Van Hoof C, Neves HP. Two-dimensional multi-channel neural probes with electronic depth control. *IEEE Trans Biomed Circuits Syst*. 2011 Oct; 5 (5):403-12. doi: 10.1109/TBCAS.2011.2162840.

17.2 Authors' other publications not related to the dissertation

- [IV]. Csercsa R, Dombovári B, Fabó D, Wittner L, Eross L, Entz L, Sólyom A, Rásonyi G, Szucs A, Kelemen A, Jakus R, Juhos V, Grand L, Magony A, Halász P, Freund TF, Maglóczky Z, Cash SS, Papp L, Karmos G, Halgren E, Ulbert I. Laminar analysis of slow wave activity in humans. *Brain*. 2010 Sep;133(9):2814-29. doi: 10.1093/brain/awq169. Epub 2010 Jul 23. PubMed PMID: 20656697;
- [V]. Grand L, Wittner L, Herwik S, Göthelid E, Ruther P, Oscarsson S, Neves H, Dombovári B, Csercsa R, Karmos G, Ulbert I. Short and long term biocompatibility of NeuroProbes silicon probes *J Neurosci Methods*. 2010 Jun 15;189(2):216-29. doi: 10.1016/j.jneumeth.2010.04.009. Epub 2010 Apr 23.
- [VI]. Fabó D, Maglóczky Z, Wittner L, Pék A, Eross L, Czirják S, Vajda J, Sólyom A, Rásonyi G, Szucs A, Kelemen A, Juhos V, Grand L, Dombovári B, Halász P, Freund

TF, Halgren E, Karmos G, Ulbert I. Properties of in vivo interictal spike generation in the human subiculum. *Brain*. 2008 Feb;131(Pt 2):485-99. Epub 2007 Dec 14.

17.3 Authors conference posters

D. Horvath, R. Fiath, B. P. Kerekes, B. Dombovari, I. Ulbert, L. Acsady, H. P. Neves, K. Seidl, O. Paul, and P. Ruther, "Thousand-channel electrode system to investigate thalamocortical interactions," Book of Abstracts, European Future Technologies (FET) Conf. 2011 (Budapest, Hungary), vol. 1, 2011.

B. Dombovari, K. Seidl, S. Herwik, T. Torfs, L. Grand, R. Cserecsa, H. Neves, O. Paul, P. Ruther, and I. Ulbert, "In vivo validation of microelectrode arrays with electronic depth control for acute recordings," Book of Abstracts, FENS Forum 2010 (Amsterdam, The Netherlands), vol. 5, p. 027.18, 2010.

T. Torfs, A. Aarts, M. Erismis, J. Aslam, R. F. Yazicioglu, C. V. Hoof, H. P. Neves, I. Ulbert, B. Dombovari, R. Fiath, B. Kerekes, K. Seidl, H. Herwik, and P. Ruther, "Two-dimensional multi-channel neural probe with electronic depth control," Proc. IEEE BioCAS Conf. 2010 (Paphos, Cyprus), pp. 198 – 201, 2010.

Fiáth R, Horváth D, Grand L, Wittner L, Dombovári B, Karmos G, Ulbert I, Cserecsa R. Laminar distribution of the spontaneous multiunit activity in the cat auditory cortex during slow wave sleep. P4-10. IBRO Workshop, Pécs, 2010

Dombovári B, Seidl K, Herwik S, Torfs T, Grand L, Cserecsa R, Paul O, Neves HP, Ruther P, Ulbert I. Acute recordings using microelectrode arrays with electronic depth control. P7-05. IBRO Workshop, Pécs, 2010

Horváth D, Grand L, Wittner L, Dombovári B, Kisban S, Herwik S, Ruther P, Neves HP, Karmos G, Ulbert I. Long term implantation of silicon-based micro probe arrays. P7-24. IBRO Workshop, Pécs, 2010

Fiáth R., Horváth D., Grand L., Wittner L., Dombovári B., Cserecsa R., Karmos G. & Ulbert I., Layer specific distribution of spontaneous multiunit activity in the cat auditory cortex in sleep and wakefulness, FENS conference, Amsterdam, 2010

K. Seidl, S. Herwik, R. Cserecsa, B. Dombovari, L. Grand, T. Torfs, H. Neves, I. Ulbert, O. Paul, and P. Ruther, "Acute recording in rat using CMOS-based high-density silicon microprobe array for electronic depth control, "Program No. 664.10/DD41. 2009. Neuroscience Meeting Planner. Chicago, IL: Society of Neuroscience., Online, 2009.

H. Neves, K. Seidl, T. Torfs, P. A. D. Maziere, G. V. Dijk, R. Csercsa, B. Dombovari, Y. Nurcahyo, C. V. Hoof, M. M. V. Hulle, G. A. Orban, O. Paul, I. Ulbert, and P. Ruther, "Supervisory software for electronic depth control microprobe arrays," NeuroMath Workshop (Advanced Methods for the Estimation of Human Brain Activity and Connectivity), March 12-13, Leuven, Belgium, 2009.

B. Dombovari, R. Csercsa, K. Seidl, P. Ruther, H. Neves, and I. Ulbert, "Electronic depth control with NeuroProbes microarrays," Book of Abstracts, 12th Meeting Hungarian Neurosci. Soc. 2009 (Budapest, Hungary), 2009.

Grand L., Dombovari B., Csercsa R., Wittner L., Magony A., Karmos G., Ulbert I., "Cortical gating of auditory information processing in sleep," Codybs Workshop, 21-25 June 2009.

R. Csercsa, B. Dombovari, L. Grand, A. Magony, L. Wittner, L. Eross, G. Karmos, I. Ulbert, "Supragranular origin of slow sleep oscillations in the human frontal lobe," Codybs Workshop, 21-25 June 2009

R. Csercsa, A. Magony, B. Dombovari, L. Grand, D. Fabo, L. Entz, L. Wittner, L. Eross, I. Ulbert, "Laminar properties of sleep slow oscillation in humans," FENS Forum Abstracts, 12-16 July 2008; 4: 160.163

Dombovári B., Grand L., Wittner L., Karmos G., Ulbert I., "Comparison of auditory information processing in sleep and anesthesia," IBRO workshop, 24-26 Jan 2008; P85

Ulbert I., Grand L., Dombovári B., Csercsa R., Magony A., Boldizsár E., Karmos G., "Evoked cortical hyperpolarization controls auditory information processing in natural non-REM sleep," SFN Conference, 14-18 Oct 2006; 239.231/G23

Ulbert I., Csercsa R., Grand L., Boldizsár E., Magony A., Dombovári B., Karmos G., "Evoked 'up' states in the cat auditory cortex," FENS Forum Abstracts, 8-12 July 2006; 3:A073.019

Grand L., Dombovari B., Boldizsar E., Karmos G., Ulbert I., "Cortical Gating of Auditory Information Processing in Sleep," FENS Forum Abstracts, 8-12 July 2006; 3:A073.6

18 References

- [1] Abeles M, Corticonics: Neural Circuits of the Cerebral Cortex, 1st ed. Cambridge University Press, 1991.
- [2] Achermann P., Borbely AA., Low-frequency (< 1 Hz) oscillations in the human sleep electroencephalogram. *Neuroscience*, 81, 213-222., 1997
- [3] Amzica F., Steriade M., Cellular substrates and laminar profile of sleep K-complex. *Neuroscience*, 82, 671-686., 1998
- [4] Amzica F., Steriade M., Disconnection of intracortical synaptic linkages disrupts synchronization of a slow oscillation. *J Neurosci*, 15, 4658-4677., 1995
- [5] Bai Q, and Wise KD. Single-unit neural recording with active microelectrode arrays. *IEEE Trans Biomed Eng* 48: 911-920, 2001.
- [6] Berenyi A, Somogyvari Z, Nagy AJ, Roux L, Long JD, Fujisawa S, Stark E, Leonardo A, Harris TD, and Buzsaki G. Large-scale, high-density (up to 512 channels) recording of local circuits in behaving animals. *J Neurophysiol* 111: 1132-1149, 2014.
- [7] Bereshpolova Y, Amitai Y, Gusev AG, Stoelzel CR and Swadlow HA, Dendritic backpropagation and the state of the awake neocortex, *J. Neurosci.*, vol. 27, no. 35, pp. 9392–9, 2007.
- [8] Berger H, Über das Elektrenkephalogramm des Menschen., *Arch. Psychiat. Nervenkr.*, vol. 87, p. 527–570, 1929.
- [9] Bhandari R, Negi S, Rieth L, Normann RA, and Solzbacher F, A novel masking method for high aspect ratio penetrating microelectrode arrays, *J. Micromech. Microeng.*, vol. 19, no. 3, p. 035004, 2009
- [10] Bilston LE, Ed., *Neural Tissue Biomechanics (Studies in Mechanobiology, Tissue Engineering and Biomaterials)*, 1st ed. Springer, 8 2011.
- [11] Blackrock Microsystems. 391 Chipeta Way Ste. G, Salt Lake City, UT 84108, USA.
- [12] Blake, H., Gerard, R., Brain potentials during sleep. *Am J Physiol*, 119, 692-703., 1937
- [13] Blanche TJ, Spacek MA, Hetke JF, and Swindale NV. Polytrodes: high-density silicon electrode arrays for large-scale multiunit recording. *J Neurophysiol* 93: 2987-3000, 2005.
- [14] Borbely, AA., A two process model of sleep regulation. *Hum Neurobiol*, 1, 195-204., 1982
- [15] Bragin A, Hetke J, Wilson CL, Anderson DJ, Engel J, Jr. and Buzsaki G. Multiple site silicon-based probes for chronic recordings in freely moving rats: implantation, recording and histological verification. *J Neurosci Methods* 98: 77-82, 2000.

- [16] Buzsaki G and Kandel A, Somadendritic backpropagation of action potentials in cortical pyramidal cells of the awake rat, *J. Neurophysiol.*, vol. 79, no. 3, pp. 1587–91, 1998.
- [17] Buzsaki G, Anastassiou CA and Koch C, The origin of extracellular fields and currents - EEG, ECoG, LFP and spikes. *Nat Rev Neurosci.* 13 (6):407-20, 2012
- [18] Buzsaki G. Large-scale recording of neuronal ensembles. *Nat Neurosci* 7: 446-451, 2004.
- [19] Campbell PK, Jones KE, Huber RJ, Horch KW, and Normann RA. A silicon-based, three-dimensional neural interface: manufacturing processes for an intracortical electrode array. *IEEE Trans Biomed Eng* 38: 758-768, 1991.
- [20] Cash SS., Halgren E., Dehghani N., Rossetti AO., Thesen T., Wang C., Devinsky O., Kuzniecky R., Doyle W., Madsen JR., Bromfield E., Eross L., Halasz P., Karmos G., Csercsa R., Wittner L., Ulbert I., The human K-complex represents an isolated cortical down-state. *Science*, 324, 1084-1087., 2009
- [21] Cham JG, Branchaud EA, Nenadic Z, Greger B, Andersen RA and Burdick JW, Semi-chronic motorized microdrive and control algorithm for autonomously isolating and maintaining optimal extracellular action potentials, *J. Neurophysiol.*, vol. 93, no. 1, pp. 570–9, 2005.
- [22] Chapin JK, Moxon KA, Markowitz RS, and Nicolelis MAL, Real-time control of a robot arm using simultaneously recorded neurons in the motor cortex, *Nat. Neurosci.*, vol. 2, no. 7, pp. 664–70, 1999.
- [23] Chauvette S., Volgushev M., Timofeev I., Origin of Active States in Local Neocortical Networks during Slow Sleep Oscillation. *Cereb Cortex.*, 2010
- [24] Chen YY, Lai HY, Lin SH, Cho CW, Chao WH, Liao CH, Tsang S, Chen YF, and Lin SY. Design and fabrication of a polyimide-based microelectrode array: application in neural recording and repeatable electrolytic lesion in rat brain. *J Neurosci Methods* 182: 6-16, 2009.
- [25] Cheung KC. Implantable microscale neural interfaces. *Biomed Microdevices* 9: 923-938, 2007.
- [26] Contreras, D., Timofeev, I., Steriade, M., Mechanisms of long-lasting hyperpolarizations underlying slow sleep oscillations in cat corticothalamic networks. *J Physiol*, 494 (Pt 1), 251-264., 1996
- [27] Cooper, R., J. Osselton, W., Shaw, J. C., *EEG Technology*, Second Edition, Butterworths, 1974
- [28] Crunelli V, and Hughes SW. The slow (<1 Hz) rhythm of non-REM sleep: a dialogue between three cardinal oscillators. *Nat Neurosci* 13: 9-17, 2010.

- [29] Crunelli V, David F, Lorincz ML, and Hughes SW. The thalamocortical network as a single slow wave-generating unit. *Curr Opin Neurobiol* 31C: 72-80, 2014.
- [30] Csercsa R, Dombovári B, Fabó D, Wittner L, Eross L, Entz L, Sólyom A, Rásonyi G, Szucs A, Kelemen A, Jakus R, Juhos V, Grand L, Magony A, Halász P, Freund TF, Maglóczy Z, Cash SS, Papp L, Karmos G, Halgren E, Ulbert I. Laminar analysis of slow wave activity in humans. *Brain*. 2010 Sep; 133 (9):2814-29. doi: 10.1093/brain/awq169. Epub 2010 Jul 23. PubMed PMID: 20656697;
- [31] Csicsvari J, Henze DA, Jamieson B, Harris KD, Sirota A, Bartho P, Wise KD, and Buzsaki G. Massively parallel recording of unit and local field potentials with silicon-based electrodes. *J Neurophysiol* 90: 1314-1323, 2003.
- [32] Csicsvari J, Hirase H, Czurko A, and Buzsaki G. Reliability and state dependence of pyramidal cell-interneuron synapses in the hippocampus: an ensemble approach in the behaving rat. *Neuron* 21: 179-189, 1998.
- [33] Delorme A, Makeig S. EEGLAB: an open source toolbox for analysis of single trial EEG dynamics including independent component analysis. *J Neurosci Methods*, 134: 9 – 21., 2004
- [34] Destexhe A., Contreras D., Steriade M., Spatiotemporal analysis of local field potentials and unit discharges in cat cerebral cortex during natural wake and sleep states. *J Neurosci*, 19, 4595-4608., 1999
- [35] Destexhe A., Hughes SW., Rudolph M., Crunelli V., Are corticothalamic 'up' states fragments of wakefulness? *Trends Neurosci*, 30, 334-342., 2007
- [36] Destexhe A., Rudolph M., Pare D., The high-conductance state of neocortical neurons in vivo. *Nat Rev Neurosci*, 4, 739-751, 2003
- [37] Drake KL, Wise KD, Farraye J, Anderson DJ, and Bement SL. Performance of Planar Multisite Microprobes in Recording Extracellular Single-Unit Intracortical Activity. *IEEE Trans Biomed Eng* 35: 719-732, 1988.
- [38] Du J, Blanche TJ, Harrison RR, Lester HA, and Masmanidis SC. Multiplexed, high density electrophysiology with nanofabricated neural probes. *PLoS One* 6: e26204, 2011.
- [39] Du J, Riedel-Kruse IH, Nawroth JC, Roukes ML, Laurent G, and Masmanidis SC. High-resolution three-dimensional extracellular recording of neuronal activity with microfabricated electrode arrays. *J Neurophysiol* 101: 1671-1678, 2009.
- [40] Entz L, Toth E, Keller CJ, Bickel S, Groppe DM, Fabo D, Kozak LR, Eross L, Ulbert I, Mehta AD., Evoked effective connectivity of the human neocortex. *Hum Brain Mapp*. 35(12):5736-53. doi: 10.1002/hbm.22581., 2014

- [41] Fee MS and Leonardo A, Miniature motorized microdrive and commutator system for chronic neural recording in small animals, *J. Neurosci. Meth.*, vol. 112, no. 2, pp. 83–94, 2001.
- [42] Franssila S, *Introduction to Microfabrication*, 2nd ed. Wiley, 2010.
- [43] Gao L., Meng X., Ye C., Zhang H., Liu C., Dan Y., Poo MM., He J., Zhang X., Entrainment of slow oscillations of auditory thalamic neurons by repetitive sound stimuli. *J Neurosci*, 29, 6013-6021., 2009
- [44] Gilletti A and Muthuswamy J, Brain micromotion around implants in the rodent somatosensory cortex, *J. Neural Eng.*, vol. 3, no. 3, pp. 189–95, 2006.
- [45] Gold C, Henze DA, Koch C and Buzsaki G, On the origin of the extracellular action potential waveform: A modeling study, *J. Neurophysiol.*, vol. 95, no. 5, pp. 3113–28, 2006.
- [46] Grand L, Pongrácz A, Vázsonyi É, Márton G, Gubán D, Fiáth R, Kerekes BP, Karmos G, Ulbert I, and Battistig G. A novel multisite silicon probe for high quality laminar neural recordings. *Sensors and Actuators A: Physical* 166: 14-21, 2011.
- [47] Haider B, Duque A, Hasenstaub AR, McCormick DA. Neocortical network activity in vivo is generated through a dynamic balance of excitation and inhibition. *J Neurosci*. 26:4535–4545, 2006
- [48] Haider B, Duque A, Hasenstaub AR, Yu Y, McCormick DA. Enhancement of visual responsiveness by spontaneous local network activity in vivo. *J Neurophysiol*. 97:4186–4202, 2007
- [49] Hajj-Hassan M, Chodavarapu V and Musallam S, NeuroMEMS: neural probe microtechnologies, *Sensors*, 8:10, 2008
- [50] Harris KD, Henze DA, Csicsvari J, Hirase H, and Buzsaki G. Accuracy of tetrode spike separation as determined by simultaneous intracellular and extracellular measurements. *J Neurophysiol* 84: 401-414, 2000.
- [51] He J., Slow oscillation in non-lemniscal auditory thalamus. *J Neurosci*, 23, 8281-8290., 2003
- [52] Heitler JW. *DataView v5: software for the display and analysis of digital signals in neurophysiology*. 2006.
- [53] Henze DA, Borhegyi Z, Csicsvari J, Mamiya A, Harris KD and Buzsaki G, Intracellular features predicted by extracellular recordings in the hippocampus in vivo, *J. Neurophysiol.*, vol. 84, no. 1, pp. 390–400, 2000.
- [54] Herwik S, Kisban S, Aarts A, Seidl K, Girardeau G, Benchenane K, Zugaro M, Wiener S, Neves HP, Paul O and Ruther P, Fabrication technology for silicon based microprobe arrays used in acute and subchronic neural recording, *Techn. Digest 19th MicroMechanics Europe Workshop (Aachen, Germany)*, pp. 57–60, 2008.

- [55] Herwik S, Kisban S, Aarts A, Seidl K, Girardeau G, Benchenane K, Zugaro MB, Wiener SI, Paul O, Neves HP and Ruther R, Fabrication technology for silicon-based microprobe arrays used in acute and sub-chronic neural recording, *J. Micromech. Microeng.*, vol. 19, p. 074008 (11pp), 2009.
- [56] Herwik S, Paul O and Ruther P, Ultrathin silicon chips of arbitrary shape by etching before grinding, *J. Microelectromech. Syst.*, vol. 20, no. 4, pp. 791–3, 2011.
- [57] Hierlemann A, Frey U, Hafizovic S and Heer F., Growing cells atop microelectronic chips: Interfacing electrogenic cells in vitro with CMOS-based microelectrode arrays, *IEEE Proc.*, vol. 99, pp. 252–84, 2011.
- [58] Hill, S. and Tononi, G., Modeling sleep and wakefulness in the thalamocortical system. *J Neurophysiol*, 93, 1671-1698., 2005
- [59] Hochberg LR, Serruya MD, Friehs GM, Mukand JA, Saleh M, Caplan AH, Branner A, Chen D, Penn RD, and Donoghue JP. Neuronal ensemble control of prosthetic devices by a human with tetraplegia. *Nature* 442: 164-171, 2006.
- [60] Hodgkin AL and Huxley AF, A quantitative description of membrane current and its application to conduction and excitation in nerve, *The Journal of Physiology*, vol. 117, no. 4, pp. 500–44, 1952.
- [61] Horton JC and Adams DL, The cortical column: A structure without a function, *Philos. Trans. R. Soc. London [Biol.]*, vol. 360, no. 1456, pp. 837–62, 2005.
- [62] <http://www.anthemion.co.uk/dialogblocks/>
- [63] <http://www.doxygen.org>
- [64] <http://www.edfplus.info>
- [65] <http://www.openmp.org/>
- [66] <http://www.wxwidgets.org>
- [67] Iber C., Ancoli-Israel S., Chesson A., Quan SF., *The AASM Manual for the Scoring of Sleep and Associated Events: Rules, Terminology and Technical Specifications*. American Academy of Sleep Medicine, Westchester., 2007
- [68] Ifft PJ, Shokur S, Li Z, Lebedev MA, and Nicolelis MA. A brain-machine interface enables bimanual arm movements in monkeys. *Sci Transl Med* 5: 210ra154, 2013.
- [69] Ji J and Wise KD., An implantable CMOS circuit interface for multiplexed microelectrode recording arrays, *IEEE J. Solid-St. Circ.*, vol. 27, pp. 433–43, 1992.
- [70] Kandel ER, Schwartz JH and Jessell TM, Eds., *Principles of neural science*, 4th ed. New York: McGraw-Hill, 2000.
- [71] Karbowski K., Hans Berger (1873-1941), *Journal of Neurology, Neurosurgery & Psychiatry* 249 (8), pp. 1130–1, doi:10.1007/s00415-002-0872-4, PMID 12420722, 2002

- [72] Karmos G, Molnar M, and Csepe V. A New Multielectrode for Chronic Recording of Intra-Cortical Field Potentials in Cats. *Physiol Behav* 29: 567-571, 1982.
- [73] Kerrigan JF., Litt B., Fisher RS., Cranstoun S., French JA., Blum DE., Dichter M., Shetter A., Baltuch G., Jaggi J., Krone S., Brodie M., Rise M., and Graves N., Electrical stimulation of the anterior nucleus of the thalamus for the treatment of intractable epilepsy, *Epilepsia*, vol. 45, pp. 346–54, 2004
- [74] Khodagholy D, Gelinias JN, Thesen T, Doyle W, Devinsky O, Malliaras GG, and Buzsaki G. NeuroGrid: recording action potentials from the surface of the brain. *Nat Neurosci* 18: 310-315, 2015.
- [75] Kim C and Wise K, A 64-site multishank CMOS low-profile neural stimulating probe, *IEEE J. Solid-St. Circ.*, vol. 31, no. 9, pp. 1230–8, 1996.
- [76] Kipke DR, Shain W, Buzsaki G, Fetz E, Henderson JM, Hetke JF, and Schalk G. Advanced neurotechnologies for chronic neural interfaces: new horizons and clinical opportunities. *J Neurosci* 28: 11830-11838, 2008.
- [77] Klein S. Thorne BM, *Biological psychology*. New York, N.Y.: Worth. ISBN 0-7167-9922-7. 2006
- [78] Korbo L, Pakkenberg B, Ladefoged O, Gundersen HJ, Arlien-Soborg P, and Pakkenberg H., An efficient method for estimating the total number of neurons in rat brain cortex, *J. Neurosci. Meth.*, vol. 31, no. 2, pp. 93–100, 1990.
- [79] Kubie JL. A Driveable Bundle of Microwires for Collecting Single-Unit Data from Freely-Moving Rats. *Physiol Behav* 32: 115-118, 1984.
- [80] Kurth S, Ringli M, Geiger A, LeBourgeois M, Jenni OG, Huber R. Mapping of cortical activity in the first two decades of life: A high-density sleep electroencephalogram study. *J Neurosci*. 30:13211–13219, 2010
- [81] Le Van Quyen M, Foucher J, Lachaux J, Rodriguez E, Lutz A, Martinerie J, Varela FJ., Comparison of Hilbert transform and wavelet methods for the analysis of neuronal synchrony. *J Neurosci Methods*. 30;111(2):83-98., 2001
- [82] Lennie P, The cost of cortical computation, *Current Biology*, vol. 13, no. 6, pp. 493–7, 2003.
- [83] Lopez CM, Andrei A, Mitra S, Welkenhuysen M, Eberle W, Bartic C, Puers R, Yazicioglu RF, and Gielen GGE. An Implantable 455-Active-Electrode 52-Channel CMOS Neural Probe. *Ieee J Solid-St Circ* 49: 248-261, 2014.
- [84] Lübke J and Feldmeyer D, Excitatory signal flow and connectivity in a cortical column: focus on barrel cortex, *Brain Structure and Function*, vol. 212, pp. 3–17, 2007.
- [85] Luczak A., Bartho P., Consistent sequential activity across diverse forms of UP states under ketamine anesthesia. *Eur. J. Neurosci.*, 36 (6), pp. 2830-8, 2012

- [86] Mann EO., Kohl MM., Paulsen O., Distinct roles of GABA(A) and GABA(B) receptors in balancing and terminating persistent cortical activity. *J Neurosci*, 29, 7513-7518., 2009
- [87] Mao BQ., Hamzei-Sichani F., Aronov D., Froemke RC., Yuste R., Dynamics of spontaneous activity in neocortical slices. *Neuron*, 32, 883-898., 2001
- [88] Márton G, Kiss M, Orbán G, Pongrácz A, and Ulbert I. A polymer-based spiky microelectrode array for electrocorticography. *Microsystem Technologies* 2014.
- [89] Massimini M, Huber R, Ferrarelli F, Hill S, and Tononi G. The sleep slow oscillation as a traveling wave. *J Neurosci* 24: 6862-6870, 2004.
- [90] Massimini, M., Ferrarelli, F., Esser, S.K., Riedner, B.A., Huber, R., Murphy, M., Peterson, M.J., Tononi, G., Triggering sleep slow waves by transcranial magnetic stimulation. *Proc Natl Acad Sci U S A*, 104, 8496-8501., 2007
- [91] McNaughton BL, Okeefe J, and Barnes CA. The Stereotrode - a New Technique for Simultaneous Isolation of Several Single Units in the Central Nervous-System from Multiple Unit Records. *J Neurosci Methods* 8: 391-397, 1983.
- [92] Mechler F, Victor JD, Ohiorhenuan I, Schmid AM, and Hu Q. Three-dimensional localization of neurons in cortical tetrode recordings. *J Neurophysiol* 106: 828-848, 2011.
- [93] Mogilner AY and Rezaei AR., Brain stimulation: current clinical indications and future prospects, *Advances in Clinical Neurophysiology*, ser. *Supplements to Clinical Neurophysiology*, M. Hallett, L. P. II, D. Schomer, and J. Massey, Eds. Elsevier, vol. 57, pp. 721–32., 2004
- [94] Molle M, Marshall L, Gais S, and Born J. Grouping of spindle activity during slow oscillations in human non-rapid eye movement sleep. *J Neurosci* 22: 10941-10947, 2002.
- [95] Moroni, F., Nobili, L., Curcio, G., De Carli, F., Fratello, F., Marzano, C., De Gennaro, L., Ferrillo, F., Cossu, M., Francione, S., Lo Russo, G., Bertini, M., Ferrara, M., Sleep in the human hippocampus: a stereo-EEG study. *PLoS One*, 2, e867., 2007
- [96] Mountcastle VB, The columnar organization of the neocortex. *Brain*, vol. 120, no. 4, pp. 701–22, 1997.
- [97] Muthuswamy J, Okandan M, Gilletti A, Baker M and Jain T, An array of microactuated microelectrodes for monitoring single-neuronal activity in rodents, *IEEE Trans. Biomed. Eng.*, vol. 52, no. 8, pp. 1470–7, 2005.
- [98] Nenadic Z and Burdick JW, Spike detection using the continuous wavelet transform, *IEEE Trans. Biomed. Eng.*, vol. 52, no. 1, pp. 74–87, 2005.
- [99] NeuroNexus Technologies. 3985 Research Park Dr. Suite 100, Ann Arbor, MI 480108, USA.

- [100] Neves HP, Torfs T, Yazicioglu RF, Aslam J, Aarts AA, Merken P, Ruther P, and Van Hoof C. The NeuroProbes Project: A Concept for Electronic Depth Control. *Ieee Eng Med Bio* 1857-1857, 2008.
- [101] Nguyen DP, Layton SP, Hale G, Gomperts SN, Davidson TJ, Kloosterman F, and Wilson MA. Micro-drive array for chronic in vivo recording: tetrode assembly. *Journal of visualized experiments: JoVE* 2009.
- [102] Nicolelis MA, and Lebedev MA. Principles of neural ensemble physiology underlying the operation of brain-machine interfaces. *Nat Rev Neurosci* 10: 530-540, 2009.
- [103] Nicolelis MA, Dimitrov D, Carmena JM, Crist R, Lehew G, Kralik JD, and Wise SP. Chronic, multisite, multielectrode recordings in macaque monkeys. *Proc Natl Acad Sci U S A* 100: 11041-11046, 2003.
- [104] Nicolelis MA. Brain-machine interfaces to restore motor function and probe neural circuits. *Nat Rev Neurosci* 4: 417-422, 2003.
- [105] Niedermeyer E, Lopes da Silva FH, *Electroencephalography. Basic Principals, Clinical Applications, and Related Fields. Fifth Edition.* London: Williams and Wilkins, 2005
- [106] Nir Y, Staba Richard J, Andrillon T, Vyazovskiy Vladyslav V, Cirelli C, Fried I, Tononi G. Regional slow waves and spindles in human sleep. *Neuron.* 70:153–169. Bhandari R 2007, 2011
- [107] Norlin P, Kindlundh M, Mouroux A, Yoshida K and Hofmann UG., A 32- site neural recording probe fabricated by DRIE of SOI substrates, *J. Micromech. Microeng.*, vol. 12, pp. 414–9, 2002.
- [108] Nunez PL, EEG. In VS Ramachandran (Ed) *Encyclopedia of the Human Brain*, La Jolla: Academic Press, 169-179, 2002
- [109] Okeefe J, and Recce ML. Phase Relationship between Hippocampal Place Units and the Eeg Theta-Rhythm. *Hippocampus* 3: 317-330, 1993.
- [110] Ozen, S., Sirota, A., Belluscio, M.A., Anastassiou, C.A., Stark, E., Koch, C., Buzsaki, G., Transcranial electric stimulation entrains cortical neuronal populations in rats. *J Neurosci*, 30, 11476-11485., 2010
- [111] Pakkenberg B and Gundersen HJG., Neocortical neuron number in humans: Effect of sex and age, *J. Comp. Neurol.*, vol. 384, no. 2, pp. 312–20, 1997.
- [112] Paxinos G, and Watson C. *The rat brain in stereotaxic coordinates.* Amsterdam; Boston: Academic Press/Elsevier, 2007.
- [113] Perlin GE, Sodagar AM and Wise KD, Neural recording front-end designs for fully implantable neuroscience applications and neural prosthetic microsystems, *Proc. 28th Ann. Int. EMBS Conf. 2006 (New York City, NY, USA)*, pp. 2982–5, 2006.
- [114] Peters A and Sethares C, Myelinated axons and the pyramidal cell modules in monkey primary visual cortex, *J. Comp. Neurol.*, vol. 365, no. 2, pp. 232–255, 1996.

- [115] Petersen, C.C., Hahn, T.T., Mehta, M., Grinvald, A., Sakmann, B., Interaction of sensory responses with spontaneous depolarization in layer 2/3 barrel cortex. *Proc Natl Acad Sci U S A*, 100, 13638-13643., 2003
- [116] Purves D, Neuroscience, 4th ed. Sinauer Associates, Inc., 2008.
- [117] Quiroga RQ. Spike sorting. *Curr Biol* 22: R45-46, 2012.
- [118] Ren JQ, Aika Y, Heizmann CW, and Kosaka T, Quantitative analysis of neurons and glial cells in the rat somatosensory cortex, with special reference to GABAergic neurons and parvalbumin-containing neurons. *Exp. Brain Res.*, vol. 92, no. 1, pp. 1–14, 1992.
- [119] Rey HG, Pedreira C, and Quiroga RQ. Past, present and future of spike sorting techniques. *Brain Res Bull* 2015.
- [120] Robert P. Vertes, Robert W. Stackman, Jr., *Electrophysiological Recording Techniques*, Humana Press, DOI: 10.1007/978-1-60327-202-5, 2011
- [121] Ros, H., Sachdev, R.N., Yu, Y., Sestan, N., McCormick, D.A., Neocortical networks entrain neuronal circuits in cerebellar cortex. *J Neurosci*, 29, 10309-10320., 2009
- [122] Ruther P, and Paul O. New approaches for CMOS-based devices for large-scale neural recording. *Curr Opin Neurobiol* 32: 31-37, 2015.
- [123] Ruther P, Herwik S, Kisban S, Seidl K, and Paul O. Recent Progress in Neural Probes Using Silicon MEMS Technology. *Ieee T Electr Electr* 5: 505-515, 2010.
- [124] Sakata, S. and Harris, K.D., Laminar structure of spontaneous and sensory-evoked population activity in auditory cortex. *Neuron*, 64, 404-418., 2009
- [125] Sanchez-Vives, M.V. and McCormick, D.A., Cellular and network mechanisms of rhythmic recurrent activity in neocortex. *Nat Neurosci*, 3, 1027-1034., 2000
- [126] Sato T, Suzuki T and Mabuchi K, A new multi-electrode array design for chronic neural recording, with independent and automatic hydraulic positioning, *J. Neurosci. Meth.*, vol. 160, no. 1, pp. 45–51, 2007.
- [127] Schubert D, Staiger JF, Cho N, Kotter R, Zilles K and Luhmann HJ, Layerspecific intracolumnar and transcolumnar functional connectivity of layer V pyramidal cells in rat barrel cortex, *J. Neurosci.*, vol. 21, no. 10, pp. 3580–92, 2001.
- [128] Schwartz AB, Cui XT, Weber D, and Moran DW, Brain-controlled interfaces: Movement restoration with neural prosthetics, *Neuron*, vol. 52, no. 1, pp. 205–20, 2006.
- [129] Seidl K, Herwik S, Torfs T, Neves HP, Paul O, and Ruther P. CMOS-Based High-Density Silicon Microprobe Arrays for Electronic Depth Control in Intracortical Neural Recording. *Journal of Microelectromechanical Systems* 20: 1439-1448, 2011.
- [130] Seidl K, Schwaerzle M, Ulbert I, Neves HP, Paul O, and Ruther P. CMOS-based high-density silicon microprobe arrays for electronic depth control in intracortical neural recording-characterization and application. *Journal of Microelectromechanical Systems* 21: 1426-1435, 2012.

- [131] Sharma AV, Wolansky T, Dickson CT. A comparison of sleeplike slow oscillations in the hippocampus under ketamine and urethane anesthesia. *J Neurophysiol.* 104:932–939, 2010
- [132] Shobe JL, Claar LD, Parhami S, Bakhurin KI, and Masmanidis SC. Brain activity mapping at multiple scales with silicon microprobes containing 1,024 electrodes. *J Neurophysiol* 114: 2043-2052, 2015a.
- [133] Steriade M, Contreras D, Curro Dossi R, and Nunez A. The slow (< 1 Hz) oscillation in reticular thalamic and thalamocortical neurons: scenario of sleep rhythm generation in interacting thalamic and neocortical networks. *J Neurosci* 13: 3284-3299, 1993a.
- [134] Steriade M, Nunez A, and Amzica F. A novel slow (< 1 Hz) oscillation of neocortical neurons in vivo: depolarizing and hyperpolarizing components. *J Neurosci* 13: 3252-3265, 1993b.
- [135] Steriade M, Timofeev I, and Grenier F. Natural waking and sleep states: A view from inside neocortical neurons. *J Neurophysiol* 85: 1969-1985, 2001.
- [136] Steriade, M. and Amzica, F., Intracortical and corticothalamic coherency of fast spontaneous oscillations. *Proc Natl Acad Sci U S A*, 93, 2533-2538., 1996
- [137] Steriade, M. and Timofeev, I., Neuronal plasticity in thalamocortical networks during sleep and waking oscillations. *Neuron*, 37, 563-576., 2003
- [138] Timofeev I and Steriade M, Low-frequency rhythms in the thalamus of intact cortex and decorticated cats, *J Neurophysiol*, vol. 76, pp. 4152-68, Dec 1996.
- [139] Timofeev, I., Grenier, F., Steriade, M., Disfacilitation and active inhibition in the neocortex during the natural sleep-wake cycle: an intracellular study. *Proc Natl Acad Sci U S A*, 98, 1924-1929., 2001
- [140] Torfs T, Aarts A, Erismis M, et al. Two-dimensional multichannel neural probes with electronic depth control. *IEEE Trans Biomed Circ Syst*; 5: 403 – 412., 2011
- [141] Tseng, K.Y., Kasanetz, F., Kargieman, L., Riquelme, L.A., Murer, M.G. Cortical slow oscillatory activity is reflected in the membrane potential and spike trains of striatal neurons in rats with chronic nigrostriatal lesions. *J Neurosci*, 21, 6430-6439., 2001
- [142] Vandecasteele M, M S, Royer S, Belluscio M, Berenyi A, Diba K, Fujisawa S, Grosmark A, Mao D, Mizuseki K, Patel J, Stark E, Sullivan D, Watson B, and Buzsaki G. Large-scale recording of neurons by movable silicon probes in behaving rodents. *Journal of visualized experiments: JoVE* e3568, 2012.
- [143] Volgushev M., Chauvette S., Mukovski M., Timofeev I., Precise long-range synchronization of activity and silence in neocortical neurons during slow-wave oscillations [corrected]. *J Neurosci*, 26, 5665-5672., 2006

- [144] Voo L, Kumaresan S, Pintar F, Yoganandan N and Sances A, Finite-element models of the human head, *Medical and Biological Engineering and Computing*, vol. 34, pp. 375–81, 1996.
- [145] Vyazovskiy, V.V., Faraguna, U., Cirelli, C., Tononi, G., Triggering slow waves during NREM sleep in the rat by intracortical electrical stimulation: effects of sleep/wake history and background activity. *J Neurophysiol*, 101, 1921-1931., 2009
- [146] Wichmann T and DeLong MR., Deep brain stimulation for neurologic and neuropsychiatric disorders, *Neuron*, vol. 52, pp. 197–204, 2006.
- [147] Wilson MA, and McNaughton BL. Dynamics of the Hippocampal Ensemble Code for Space. *Science* 261: 1055-1058, 1993.
- [148] Wise KD, Angell JB, and Starr A. An integrated-circuit approach to extracellular microelectrodes. *IEEE Trans Biomed Eng* 17: 238-247, 1970.
- [149] Wise KD, Sodagar AM, Yao Y, Gulari MN, Perlin GE, and Najafi K. Microelectrodes, microelectronics, and implantable neural microsystems. *P Ieee* 96: 1184-1202, 2008.
- [150] Wolansky T, Clement EA, Peters SR, Palczak MA, Dickson CT. Hippocampal slow oscillation: A novel eeg state and its coordination with ongoing neocortical activity. *J Neurosci*. 26:6213–6229, 2006
- [151] Wolpaw JR, Birbaumer N, McFarland DJ, Pfurtscheller G, and Vaughan TM, Brain-computer interfaces for communication and control, *J. Clin. Neurophysiol.*, vol. 113, no. 6, pp. 767–91, 2002.
- [152] Wolpaw JR, Loeb GE, Allison BZ, Donchin E, do Nascimento OF, Heetderks WJ, Nijboer F, Shain WG, Turner JN. BCI Meeting 2005--workshop on signals and recording methods. *IEEE Trans Neural Syst Rehabil Eng*. 14(2):138-41., 2006.
- [153] Yao Y, Gulari MN, Wiler JA and Wise KD, A microassembled low-profile three dimensional microelectrode array for neural prosthesis applications, *J. Microelectromech. Syst.*, vol. 16, no. 4, pp. 977–88, 2007.
- [154] Yip S, Ip JK, and Sastry BR. Electrophysiological actions of hemoglobin on rat hippocampal CA1 pyramidal neurons. *Brain Res* 713: 134-142, 1996.
- Zhang L, Yang K and King A, Comparison of brain responses between frontal and lateral impacts by finite element modeling. *J. Neurotrauma*, vol. 18, no. 1, pp. 21–30, 2001.